Fishing for answers: Investigating Fibrodysplasia Ossificans Progressiva using a novel adult zebrafish model

A thesis submitted by

Melissa LaBonty

in partial fulfillment of the requirements for the degree of

PhD

in

Cell, Molecular, and Developmental Biology

Tufts University

Sackler School of Graduate Biomedical Sciences

May 2018

Adviser: Pamela Yelick, PhD

Abstract

Fibrodysplasia Ossificans Progressiva (FOP) is a rare, autosomal dominant genetic disorder in humans characterized by the gradual ossification of fibrous tissues, including skeletal muscle, tendons, and ligaments. In humans, activating mutations in the Type I BMP/TGFβ family member receptor, ACVR1, are associated with FOP. Zebrafish acvr1l, previously known as alk8, is the functional ortholog of human ACVR1. The objective of this work is to create and characterize the first adult zebrafish model for FOP, providing a useful tool to study the development and progression of FOP-like symptoms. Constitutively active mutations in zebrafish acvr1l cause early lethal defects. Therefore, to study roles for activating acvr1l mutations in adult zebrafish, gateway cloning was used to create a vector containing the *hsp70l* heat shock promoter driving the expression of mCherry-tagged constitutively active Acvr1l (Q204D). Constructs were injected into single cell stage BMP response element reporter (Bre:GFP) zebrafish to create stable *Tg(Bre:GFP); Tg(hsp70l:acvr1l_Q204D-mCherry)* lines. Beginning at 2 weeks post fertilization, developmentally staged transgenic animals were subjected to daily one-hour heat shock treatments (3 weeks to 12 months) to induce Acvr1l^{Q204D} expression. Micro-CT was used on whole animals to confirm FOP-like skeletal defects. Acvr1l^{Q204D}-expressing animals displayed HO formation, abnormal spinal curvature, vertebral fusions, and malformation of pelvic fins, as compared to heat shocked *Tg(Bre:GFP)* animals and non-heat shocked controls. Histological stains (Safranin O and Hall and Brunt's Quadruple Stain) were used to confirm the presence of cartilaginous proteoglycans and mineralized tissue formation in the HO lesions. As injury is a known trigger for HO development in human FOP patients, several injury models were tested on

Acvr1l^{Q204D}-expressing animals to induce the formation of reliable, replicable HO. Activin A injection, cardiotoxin injection, and caudal fin clip injuries were all developed. None of these methods resulted in HO formation at the site of injury. However, cardiotoxin injected and caudal fin clipped animals did develop HO at distant sties, including the body cavity and along the spine. In summary, these results suggest that heat-shocked Acvr1l^{Q204D}-expressing adult zebrafish provide an informative model for human FOP, but further work is needed to identify an effective method for inducing reliable site-directed HO.

Dedication

First and foremost, this entire thesis and all of the work that has culminated in the receipt of my doctoral degree is dedicated to the love of my life, Alexander Mann. This wonderful person has spent years gently reminding and convincing me of my strengths, abilities, and self-worth. He has read countless drafts, providing comments on grammar, flow, and (to the best of his ability) content. He has been my sounding board for career considerations, workplace difficulties, mentor-mentee relationships, scientific troubleshooting, and everything else in between. He offered just the support I needed when things got tough during my second year (and my fourth year). He is prepared and excited to lovingly follow me in pursuit of my perhaps crazy, probably competitive, definitely rewarding career goals. I love the generous, strong, focused person that I have become as a result of his presence and support in my life. I hope that he is as proud of the work I have done and the path that I have chosen as I am.

I would also like to dedicate this work to my parents, James and Mary LaBonty, who have always been my greatest fans. Perhaps it is because they are both science-minded individuals themselves, but I never encountered a moment of hesitation or resistance toward any of my goals and ambitions for my career. I truly appreciate the work that they have done and the sacrifices that they have made in life to provide me with the opportunities I have had to succeed.

Last, I would like to dedicate this work to my many amazing friends, and in particular Carrie Hui and Joslyn Mills. Carrie and I have been there for each other from the very first day of grad school. We were study buddies in first year, bridesmaids for one another during the middle years, and have turned into each other's cheerleaders as we

wrap up our thesis work within the same month. While our paths will head in different directions after graduation, hers out of academia and into consulting, mine towards academic research and teaching, we are sure to remain lifelong friends. Joslyn and I finally crossed paths later in our years at Sackler, despite having many of the same connections and participating in many of the same teaching and outreach programs. It is not often that you meet someone who shares your passions and career goals, but I have found that person in Joslyn and it has been so comforting and motivating to have her navigating this journey by my side. I look forward to maintaining a wonderful, fruitful relationship with her, both personally and professionally.

Acknowledgments

I would like to begin by acknowledging Dr. Pamela C. Yelick, my thesis advisor and mentor. By the end of my first rotation at Sackler, Pam and I quickly developed a strong relationship built on mutual respect and trust. She provided an environment for me in her lab where I could develop my confidence, build upon my mentoring skills, and come into my own as an academic scientist. I am incredibly grateful to her for the guidance and support that she has provided over the years – it has been truly invaluable.

I would also like to acknowledge the members of my committee, Dr. Leif Oxburgh, Dr. Cliff Rosen, Dr. Laura Liscum, and Dr. Aris Economides, for their encouragement and suggestions during my time at Sackler. Leif, Cliff, and Aris have each provided the scientific advice to steer my experiments in the most fruitful directions, resulting in two elegant and respectable publications and a third on the way. Laura has acted as a personal advocate for my academic teaching interests, providing me with information and opportunities to uncover my passion for teaching and develop strong and clear career goals.

I would like to acknowledge the faculty and staff of the Sackler School, and in particular the members of the Cell, Molecular, and Developmental Biology program. I have not had a perfectly linear, unremarkable path through my graduate program, but I have had the support of the school throughout my journey and it has made all the difference in my success. Dr. John Castellot and Dr. Beverly Rubin provided much-needed guidance during my early years in the program, while Dr. Ira Herman has truly led by example during my final years. Associate Dean Kathryn Lange helped me to navigate around a number of obstacles during my graduate career.

It is my pleasure to acknowledge the many wonderful coworkers that I have worked with during my time in the Yelick lab. Dr. Chengtian Zhao gave me the kindest, truest crash course in being an academic researcher during my first rotation in the Yelick lab at Sackler. Dr. Viktoria Andreeva helped me to establish my presence and project once I joined the Yelick lab. John Lyons was a true comrade-in-arms, teaching me everything I could possibly need to know about fish husbandry and fish system maintenance, all while regaling me with stories of many exciting adventures from his still young life. Nicholas Pray assisted me in processing and analyzing an incredible number of samples for this work. Alex Cintolo has graciously and admirably taken over the job of maintaining our precious fish and provided some much needed companionship during the final months of my graduate career. All of the weekend and holiday fish feeders over the years have helped to make sure that our precious fish get fed 365 days of the year (science never sleeps!). The members of the tissue engineering lab, Elizabeth Smith, Weibo Zhang, and Nelson Monteiro, have offered excellent scientific and personal advice.

Additionally, I have had the amazing, though also sometimes daunting, opportunity to mentor a large number of students and interns from all walks of life during my years at Sackler. I would like to acknowledge them all here: Evan Brooks, Nicole Fisher, Sophie Chase, Kei Thurber, Trish Hare, Shaina Colón, Shirin Shabahang, Caroline Banevicius, YooJin Yoon, Emily Chen, Lauren Weinstock, Annabel Azziz, Michael Chen, and Andrade Hendricks. Each and every one of them has helped me to grow as a scientist and as a person. They have inspired me with their maturity, motivation, and enthusiasm. They have exposed me to the differences in experience that

each student faces and have moved me to dedicate a meaningful portion of my time as a scientist to remedying some of the historical disparities in academic science research.

I would also like two acknowledge two amazing figures in my academic career, Dr. Erin Cram and Dr. Angela Seliga. I would not have even applied to graduate school if it weren't for the encouragement of my former boss, Erin. She guided me through my evolution from a timid, insecure recent college graduate into a well-trained, professional, confident graduate school applicant during my three years as a technician in her lab. She continues to be an incredible mentor and I consider myself so fortunate to have crossed paths with her so early in my career. I found my calling in science teaching through the relationship I developed with Dr. Angela Seliga. She has provided me the opportunity to try my hand at everything from instruction to curriculum design and given me the tools to succeed at every step along the way. I am infinitely grateful for her presence in my life. Both Angela and Erin serve as models of exactly the kind of scientist and mentor I aim to be for future students and mentees.

Finally, I would like to acknowledge the funding sources that supported this work, granted by the NIH/NIDCR (R01DE018043, PCY, and R21AR065761, PCY) and the NSF (GRFP NS9344, ML).

Table of Contents

List of Tables

List of Figures

List of Copyrighted Materials Produced by the Author

1. M. LaBonty, P. C. Yelick, Animal models of fibrodysplasia ossificans progressiva, *Dev. Dyn.* **247**, 279–288 (2018).

2. M. LaBonty, N. Pray, P. C. Yelick, A Zebrafish Model of Human Fibrodysplasia Ossificans Progressiva, *Zebrafish* **14**, 293–304 (2017).

List of Abbreviations

Ab – Antibody
ABC – Avidin-Biotin Complex
ActRII/ActRIIB – Activin A Receptor Type 2/Activin A Receptor Type 2B
ACVR1/Acvr1l – Activin A Receptor Type 1/Activin A Receptor Type 1-like
ALK2 – Activin Receptor-like Kinase 2
Alk8 – Activin Receptor-like Kinase 8
BMP – Bone Morphogenetic Protein
bp – base pair
Bre – BMP Response Element
CD19 – Cluster of Differentiation 19
Col I – Collagen I
Col II – Collagen II
COP – Circulating Osteogenic Precursor
CRISPR – Clustered Regularly Interspaced Short Palindromic Repeats
CTX – Cardiotoxin
DAB – 3,3'-diaminobenzidine
DMSO – Dimethyl Sulfoxide
dpf – days post fertilization
dpi – days post-injury
ENU – N-ethyl- nitroso-urea
FOP – Fibrodysplasia Ossificans Progressiva
FoxD1 – Forkhead Box D1
GFP – Green Fluorescent Protein
GS – Glycine-serine
H&E – Hematoxylin & Eosin
HBQ – Hall's and Brunt's Quadruple (Stain)
HIF-1α – Hypoxia-inducible Factor 1 alpha
HO – Heterotopic Ossification
hpf – hours post fertilization
hpi – hours post-injury
HRP – Horseradish Peroxidase
Hsp70/hsp70l – Heat shock Protein, 70 kDa/heat shock protein, 70 kDa, like
IACUC – Institutional Animal Care and Use Committee
IHC – Immunohistochemistry
KOH – Potassium Hydroxide
LCK – Lymphocyte-specific Protein Tyrosine Kinase
LG02 – Linkage Group 2
Lyz – Lysozyme
Micro-CT/μCT – Micro-computed Tomography
MRI – Magnetic Resonance Imaging
Mx1 – Myxovirus Resistance 1
Myf5 – Myogenic Factor 5
NSAID – Non-steroidal Anti-inflammatory Drug
PBS – Phosphate-buffered Saline

PET/CT – Positron Emission Tomography/Computed Tomography
pSmad2 – phosphorylated Smad2
PVDF – Polyvinylidene Fluoride
RA – Retinoic Acid
RARγ – Retinoic Acid Receptor gamma
rh – recombinant human
R-Smad – Regulatory Smad
RT – Room Temperature
Sax – Saxaphone
Scx – Scleraxis
TBST – Tris-buffered Saline with Tween-20
TGFβ – Transforming Growth Factor beta
Tie2 – Tunica Interna Endothelial Cell Kinase
vWF – von Willebrand Factor
wpi – weeks post-injury
WT - Wildtype
ZIRC – Zebrafish International Resource Center

Chapter 1: Introduction

1.1 Introduction to FOP

Fibrodysplasia Ossificans Progressiva (FOP) is a rare human skeletal disease classically characterized by the widespread, progressive, and irreversible formation of heterotopic ossification (HO) *(1-5)*. Heterotopic ossification (HO) is the process of bone formation outside of the normal skeleton *(6)*. FOP patients develop HO, and a number of additional phenotypes, due to mutations in a single gene, ACVR1 *(7, 8)*. These mutations result in constitutive activation of ACVR1, a type I Transforming Growth Factor β/Bone Morphogenetic Protein (TGFβ/BMP) receptor, and overactivation of BMP signal transduction pathways *(9-13)*.

1.1.1 Pathology of FOP

There are two features of FOP in humans that are considered to be classical hallmarks of the disease: malformation of the big toes and progressive HO formation *(2, 4, 7, 8)*. Nearly all patients with FOP present with big toe malformations at birth *(4, 7, 8)*. As they get older, patients begin to develop HO lesions within fibrous tissues, including skeletal muscle, ligaments, and tendons (Figure 1.1A) *(2, 4, 8)*. Notably, the diaphragm, tongue, and cardiac and smooth muscle remain untouched by FOP lesions *(4)*.

The majority of FOP patients form HO lesions within the first decade of life *(14-16)*. Lesion formation typically begins in axial and proximal regions, such as the neck and upper back, then radiates into appendicular and distal regions during adolescence and adulthood *(16)*. Nearly all patients experience progressively limited mobility into adulthood due to HO formation and joint ankylosis *(16)*. The median age of survival is 40 years and the most common cause of death in patients is thoracic insufficiency syndrome *(17)*. While the trend of disease manifestation is progressive in all FOP patients, the rate

of progression can vary quite dramatically among patients, with a subset of individuals showing slowed or minimal disease progression and extended lifespans *(16)*.

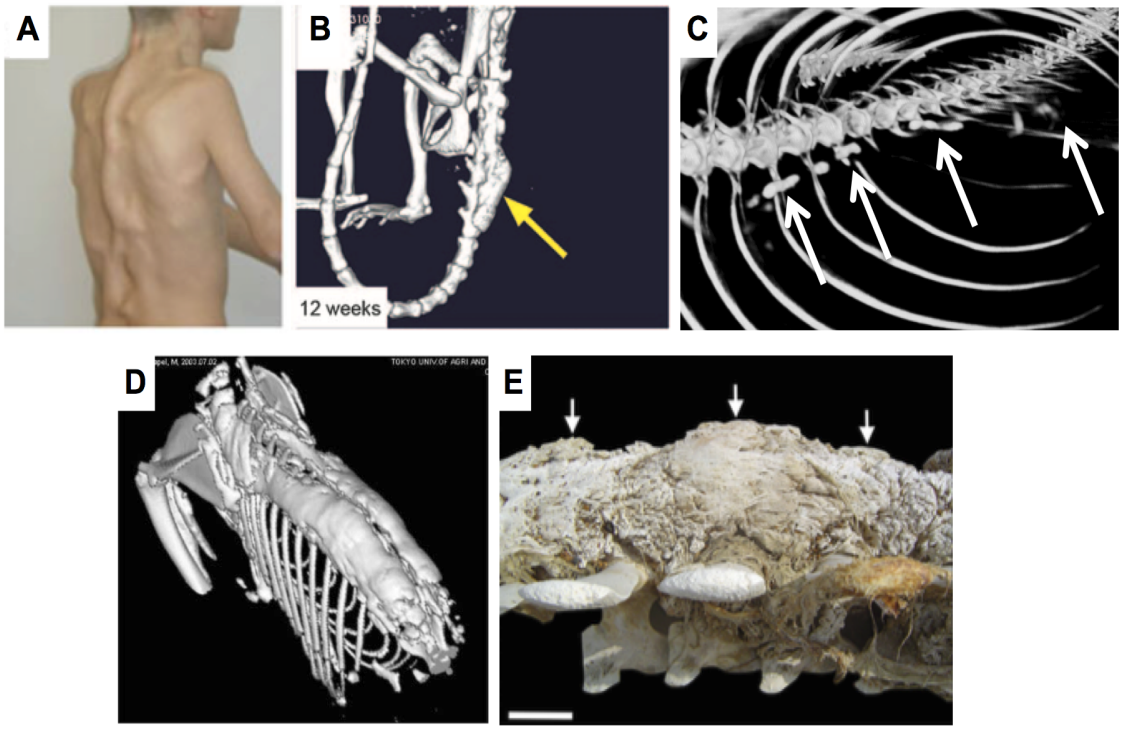

Figure 1.1. FOP in animal models. Visualization of the classic FOP phenotype, HO, in (A) human *(8)*, (B) mouse conditional-on knock-in *ACVR1*^{R206H} model *(18)*, (C) zebrafish heat-shock-inducible *Acvr1l*^{Q204D} model, (D) cat *(19)*, and (E) whale *(20)*. Reprinted with permission from M. LaBonty, P. C. Yelick, Animal models of fibrodysplasia ossificans progressiva, *Dev. Dyn.* **247**, 279–288 (2018) *(21)*

A number of other phenotypes associated with FOP are common but highly variable. These include osteochondromas (>90% of patients), cervical spine malformations (>80% of patients), chronic neurological symptoms (~50% of patients), and thumb malformations (~50% of patients) *(8, 22)*. Among individual cases, patients have been documented with atypical characteristics such as loss of digits, growth retardation, aplastic anemia, cataracts, and retinal detachment *(8)*.

1.1.2 Genetics of FOP

FOP is estimated to affect about 3,500 people worldwide, or 1 in every 2 million live births, with 685 classically-affected patients identified as of 2016 *(16)*. The disease predominantly arises through sporadic (noninherited) mutation, though it can also be inherited in an autosomal dominant fashion *(1-5)*. All individuals with FOP carry an activating mutation in one copy of the gene encoding ACVR1 (also known as ALK2) *(7, 8)*. Nearly 90% of cases display the classic p.R206H mutation *(8)*. The remaining ~10% of patients carry atypical mutations that often result in a number of the rare or atypical phenotypes described above *(4, 8)*.

1.1.3 ACVR1, a Type I TGFβ/BMP receptor

ACVR1 is one of the seven Type I TGFβ/BMP receptor family members *(23-25)*. In TGFβ/BMP signal transduction, a dimer of one of the more than 30 TGFβ superfamily of extracellular ligands binds to a Type II receptor dimer, then recruits a type one receptor dimer to complete a tetrameric receptor complex *(25)*. The ligand-receptor complex is activated by transphosphorylation of the Type I receptor intracellular glycine-serine (GS) domains by the Type II receptors *(23-25)*. The activated Type I receptors can then phosphorylate their downstream cytoplasmic Smad signaling partners, which include the regulatory Smads (R-Smads), Smad1, Smad2, Smad3, Smad5, Smad7, Smad8 and Smad9 *(23-25)*. The phosphorylated R-Smads then associate with the Co-Smad, Smad4, and subsequently translocate to the nucleus where they can act as transcription factor complexes to mediate gene expression *(23-25)*.

TGFβ/BMP signaling pathways are involved in a wide range of cellular and developmental processes, including early embryonic axis formation, germ-layer

specification, gastrulation, left-right asymmetry, and organogenesis [Reviewed in *(26)*]. Endochondral ossification, one of the natural pathways for bone formation, is uniquely regulated by the BMP and TGFβ signaling pathways *(27)*. ACVR1 associates with a specific subset of ligands, Type II receptors, and downstream Smad signaling partners to propagate BMP signaling that promotes endochondral ossification (Figure 1.2A). ACVR1 forms tetrameric receptor complexes with ActRII and ActRIIB *(23, 28)*. BMP6 and BMP7 display the strongest ligand binding interactions with the ActRII/ACVR1 receptor complex *(28, 29)*, while BMP2 and BMP4 can bind to the receptor complex to a lesser degree *(18, 23, 29)*. Once formed, the ligand-receptor complex signals through Smad1/5/8 to promote the gene expression required for endochondral ossification *(28, 30)*. Activin A, an important activator of TGFβ-mediated inflammation (Figure 1.2A) *(31)*, is another ligand that is capable of binding to the ActRII/ACVR1 receptor complex, but instead acts as a competitive inhibitor of ACVR1-mediated signaling *(18, 32)*. This inhibition may be important for blocking undesired endochondral ossification during a normal injury response (Figure 1.2A).

Mutations found in ACVR1 that are associated with FOP all cause abnormal constitutive activation of BMP signaling. The classical p.R206H mutation, as well as the known variant p.Q207E and the artificial mutation p.Q207D, are all located within the GS domain of ACVR1 (Figure 1.2B) *(8, 13, 33)*. A number of other FOP-associated variant mutations are found in the both the GS domain and the kinase domain *(8, 29)*. Each of these mutations confers a structural change to the receptor conformation, resulting in both altered ligand specificity *(13, 18, 34)* and constitutively active ligand-independent signaling *(35-37)*. Specifically, Activin A switches roles from a competitive

inhibitor to an activator of ACVR1^{R206H}-mediated BMP signaling (Figure 1.2A) *(18, 34)*. This aberrant signal activation has been directly linked to the endochondral ossification seen in HO lesions in FOP mouse models *(18, 35, 38)*.

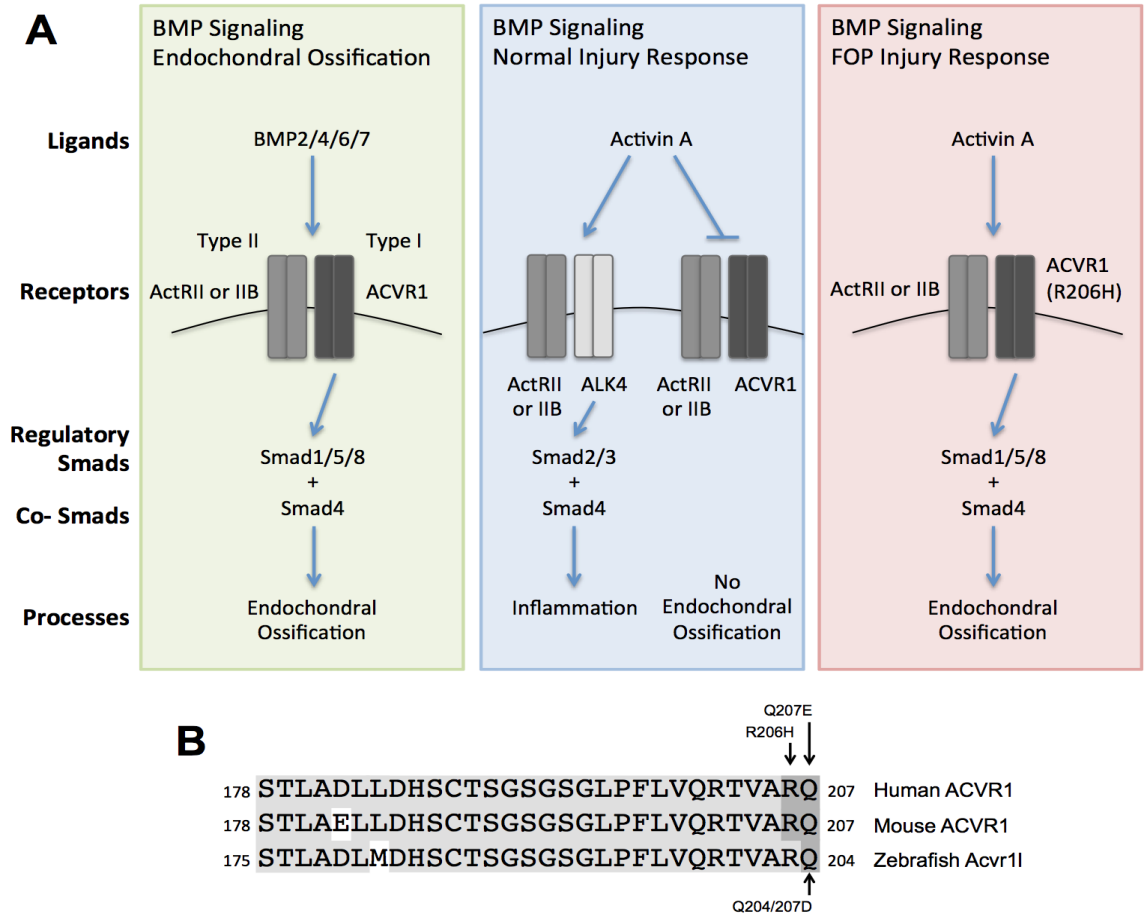

Figure 1.2. Constitutive activation of ACVR1 promotes aberrant BMP signaling. (A) Diagram of signaling through ACVR1 leading to HO development. (B) Comparison of the GS domain of each ACVR1 homolog, with human FOP variants p.R206H and p.Q207E noted, as well as mouse p.Q207D, p.R206H, and zebrafish p.Q204D, each used in respective FOP models. Reprinted with permission from M. LaBonty, P. C. Yelick, Animal models of fibrodysplasia ossificans progressiva, *Dev. Dyn.* **247**, 279–288 (2018) *(21)*

1.1.4 FOP Lesion Progression

In FOP, lesions are formed in what are referred to as 'flare-ups' *(39)*. A flare-up is described as a two-stage process of explosive inflammation leading to fibrous tissue degradation and the subsequent endochondral ossification that occurs in the wake of the tissue destruction *(39)*. Physical injury, viral infection, surgical procedures, and intramuscular injections, including immunizations, can all prompt the initial inflammation of a flare-up *(4, 40, 41)*. During this initial phase, inflammatory cells, including lymphocytes, macrophages, and mast cells, rush to the site of the lesion *(42-44)*. While this occurs in normal tissues as well, the cellular response is amplified in FOP. The inflammatory cells drive the degradation of the damaged muscle tissue, and appear to also play a critical role in producing angiogenic factors and recruiting fibroproliferative cells *(42-44)*. Interestingly, immunosuppression in mouse models of FOP and in a human FOP patient resulted in abolition of HO formation, suggesting an indispensible role for the inflammatory phase in lesion development *(45, 46)*.

During the second phase of HO formation, a resident pool of mesenchymal stem cells at the site of inflammation and degradation undergoes the BMP-mediated process of endochondral ossification to generate heterotopic bone *(39)*. The mesenchymal stem cell population is believed to have numerous origins, including but not limited to *Scx*+ tendon progenitor cells *(47)*, bone-marrow-derived muscle-resident *Mx1*+ cells *(47)*, *Glast*-expressing cells *(48)*, *Tie2*+ endothelial cells *(49-51)*, and circulating osteogenic precursor (COP) cells *(52)*.

1.1.5 Current Treatments

There is no cure for FOP. Prenatal testing for the disease is not currently available and, given the rarity of the disease, is not likely to become routine *(4)*. In addition, the disease rarity and variability in the severity of phenotypes and the rate of disease progression often result in delayed or misdiagnosis and contraindicated exacerbating medical procedures, such as surgical excisions *(4, 53)*. Once a diagnosis of FOP has been made, historically, treatment has been palliative, involving drug therapies such as glucocorticoids to decrease inflammation and NSAIDs to alleviate pain *(2, 4)*. Surgical procedures must be avoided as they provoke additional HO formation *(4)*.

Nearly 40 years ago, Pacifici and colleagues demonstrated that retinoic acid signaling acts as a strong and specific inhibitor of chondrogenesis *(54)*. More recently, researchers have demonstrated that activation of retinoic acid signaling by treatment with the retinoic acid receptor gamma (RARγ) agonist palovarotene can prevent HO formation in FOP mouse models *(55, 56)*. Based on these results, palovarotene has been moved into a National Institutes of Health-supported clinical trial to assess its ability to prevent HO formation in human FOP patients during and following flare-ups. Preliminary data from Phase 2 of the clinical trial show promising results: palovarotene treatment reduced new HO incidence in FOP patients by 50% and new HO volume by 70% (http://www.prnewswire.com/news-releases/phase-2-part-a-open-label-extension-trial-of-palovarotene-for-treatment-of-patients-with-fibrodysplasia-ossificans-progressiva-continues-positive-trends-300429975.html).

1.2 Animal Models of FOP

There is a fundamental need for animal models of FOP in which to study mechanisms of disease progression given that investigative surgical procedures in human FOP patients exacerbates HO formation *(4)*. Spontaneous cases of FOP have been described in many animals, including numerous instances in cats (Figure 1.1D) *(19, 57-60)*, dogs *(61)*, pigs *(62)*, and even a southern right whale (Figure 1.1E) *(20)*. In each of these cases, specimens presented with progressive and substantial HO development, and in some cases osteochondromas and vertebral fusions. Nearly all of these cases were described prior to the identification of *ACVR1* as the causative gene for human FOP, so none have been corroborated with molecular data to confirm the presence of activating mutations in respective *ACVR1* orthologs in these animals.

ACVR1 protein orthologs can be found as early in evolutionary history as the invertebrate class Insecta, including the *D. melanogaster* (fruit fly) protein Saxophone (Sax) *(63, 64)*. Among vertebrates, human ACVR1 and mouse ACVR1 are 98% identical *(8)*, while human ACVR1 and zebrafish Acvr1l are 69% identical *(65)*. Of note, the intracellular domains of ACVR1, the GS domain and the kinase domain, are 85% identical between human ACVR1 and zebrafish Acvr1l *(65)*. This conservation suggests preservation of protein function and provides validation for the study of ACVR1 function and dysfunction in animal models.

1.2.1 Fruit fly model

The fruit fly ortholog of human ACVR1, Sax, was first characterized in 1994 in a series of studies to identify receptors responsive to the fruit fly BMP-2/BMP-4 ortholog Decapentaplegic (Dpp) *(63, 66-68)*. Signaling through Sax is critical for dorsal

ectodermal patterning *(63, 66-71)* and for imaginal disk development leading to adult appendage formation *(63, 67, 68, 72, 73)*. The TGFβ/BMP signaling pathway is so evolutionarily well-conserved that human BMP ligands can serve as functional substitutes for their fruit fly counterparts *(63, 74)*. Thus researchers have reasoned that studying the basic mechanisms behind TGFβ/BMP signaling in development in the fruit fly could have important implications in vertebrate systems.

Since the discovery of *ACVR1* as the causative gene for human FOP, researchers have focused their work in fruit flies on the importance of the formation of tetrameric BMP receptor complexes. Fruit flies carrying the gain of function allele p.G412E in Sax are maternal effect lethal in a dosage dependent manner that suggests Sax^{G412E} participates in signaling complexes that promote overactive BMP signaling during development *(64)*. Mutations in this same residue have been found in FOP patients *(8)*. Indeed, when fruit flies carry the classical p.R206H FOP mutation, over activation of BMP signaling is dependent on type II receptor association, and is ligand-independent *(36)*.

1.2.2 Mouse models

Mouse ACVR1 (previously known as Tsk7L, Alk2, and ActR-I) was first cloned in 1993, and characterized for its ability to associate with Type II TGFβ receptors and bind a number of TGFβ family ligands, including TGFβ itself and activin, *in vitro* {Ebner:1993wb}. Studies of ACVR1-mediated BMP signaling in the mouse have revealed roles in embryonic gastrulation *(75, 76)*, neural crest cell differentiation *(77, 78)*, germ cell development *(79)*, and lens development *(80, 81)*. Given that ACVR1 is indispensible for so many aspects of mouse embryonic development, and that loss or over

activation of ACVR1 causes embryonic or perinatal lethality *(38, 75, 76)*, subsequent work on adult mouse models of FOP have focused on the use of chimeric/mosaic animals, or have taken advantage of various methods of conditional gene expression, most commonly using Cre-Lox recombination.

1.2.2.1 *ACVR1^{Q207D}* Models

The first mouse model expressing constitutively active ACVR1, through Cre-Lox-inducible overexpression *ACVR1^{Q207D}*, was generated and studied prior to the discovery of *ACVR1* as the causative gene for FOP *(82)*. Although it is now known that the p.Q207D mutation in ACVR1 is not a naturally occurring mutation found in human FOP patients, this mutation does confer constitutive activation of the ACVR1 receptor *(83)*, similar to, though more severe than, the FOP-associated mutations p.R206H and p.Q207E *(13)*. Through these experiments, it was determined that even mild, ubiquitous overexpression of ACVR1^{Q207D} promotes excessive BMP signaling and compromises embryonic development *(82)*. The authors did not investigate the role of ACVR1^{Q207D} in later development at that time.

Since the discovery that all FOP patients carry constitutively activating mutations in *ACVR1*, a number of groups have used the ACVR1^{Q207D}-expressing mouse to model FOP. Yu and colleagues bypassed the embryonic lethality of the original model through the use of two methods: 1) directed injection of adenoviral Cre recombinase into the left hindlimb to induce localized ACVR1^{Q207D} expression; 2) mating with animals carrying tamoxifen-inducible Cre-recombinase to induce global ACVR1^{Q207D} expression *(33)*. In the localized hindlimb model, ACVR1^{Q207D}-expressing mice developed decreased mobility and bony calluses at the site of injection within 30 days. In contrast, mice

globally expressing ACVR1^{Q207D} did not develop detectable HO within 60 days of tamoxifen induction. Interestingly, these animals did develop bony calluses as a result of control adenoviral injection after tamoxifen induction, indicating that inflammation or injury is required to induce heterotopic ossification in the *ACVR1^{Q207D}* background *(33)*.

Continued work with the ACVR1^{Q207D} mouse model confirmed previous results in the fruit fly model *(36, 64)*, demonstrating that ACVR1^{Q207D} requires complex formation with Type II receptors in order to promote ligand-independent BMP signal transduction *(35)*. Furthermore, the first in vivo assessments of the HO-inhibiting potential of the RARγ agonist palovarotene were conducted in the ACVR1^{Q207D} mouse model *(55)*. Researchers found that delivery of palovarotene protected against the formation of HO by reducing the overactivation of BMP signaling caused by ACVR1 constitutive activation *(55)*. The ACVR1^{Q207D} mouse model has also recently been used to establish an indispensible role for Hypoxia-inducible factor (HIF)-1α-mediated hypoxia in the early stages of HO lesion formation, identifying an additional therapeutic target for FOP *(84)*.

1.2.2.2 *ACVR1^{R206H}* Models

In recent years, researchers have endeavored to generate a mouse model harboring the classical FOP mutation, p.R206H. Chakkalakal and colleagues were the first to generate such a model, using homologous recombination to introduce the R206H mutation at the endogenous murine *Acvr1* locus *(38)*. As endogenous expression of ACVR1^{R206H} in mice causes perinatal lethality, chimeric animals with 70-90% mutant cells were used to study ACVR1^{R206H} expression in adult mice. The chimeric mice develop classic FOP features, including hind limb digit malformation, joint fusions, and

extensive HO development. In addition, the chimeric mice form substantial HO in response to muscle injury *(38)*.

Experiments have also been conducted using mesenchymal progenitor cell lines established from chimeric ACVR1$^{R206H/+}$ mice *(12)*. Using these cells, researchers have demonstrated that ACVR1^{R206H} is necessary, though not sufficient on its own, to promote chondrogenesis *in vitro* and HO formation *in vivo (12)*. BMP stimulation is required to provide the initial activation of ACVR1^{R206H}, suggesting that ACVR1$^{R206H/+}$ cells exhibit an initial ligand dependence to promote BMP signaling, that subsequently switches to ligand-independent constitutive activation after stimulation *(12)*.

Another FOP mouse model, this time utilizing a Cre-dependent conditional-on knock-in system to express the *Acvr1*^{R206H} allele at the endogenous locus, was created to bypass the perinatal lethality of the first ACVR1^{R206H} mouse model *(18)*. Using the conditional-on ACVR1^{R206H} model, Hatsell and colleagues demonstrated the progressive development of HO at many of the same sites commonly affected in human FOP patients (Figure 1.1B). It is important to note that this model was used to identify a role for activin A in the aberrant activation of ACVR1^{R206H}. Wheras activin A normally acts as an inhibitor of ACVR1, the p.R206H mutation confers a gain-of-function activity that permits activin A-mediated activation of ACVR1. Activin A delivery in the conditional-on ACVR1^{R206H} mouse leads to HO development, an effect that can be abolished by activin A-blocking antibodies *(18)*. This novel role for activin A in the activation of ACVR1^{R206H} was also observed in human FOP patient-derived induced mesenchymal stromal cells *(34)*.

Further studies utilizing the conditional-on ACVR1^{R206H} mouse model have investigated therapeutic approaches for FOP *(56)* and have generated the first natural history of developing HO lesions *(85)*. Following the finding that the RARγ agonist palovarotene could inhibit HO development in the ACVR1^{Q207D} mouse model *(55)*, Chakkalakal and colleagues sought to demonstrate the same potent inhibition in mice carrying the FOP-associated mutation, p.R206H. They showed that prenatal delivery of palovarotene to ACVR1^{R206H}-expressing mice not only reduced HO lesion formation, but also rescued malformations of the skeleton *(56)*. Very recently, Upadhyay and colleagues used a combination of MRI, Micro-CT, and PET/CT imaging techniques to track the development and progression of HO lesions in the conditional-on ACVR1^{R206H} mouse model *(85)*. These tracking modalities demonstrated that activin A, the aberrant activator of ACVR1^{R206H}, is required not only for the formation of new HO lesions, but also for the sustained growth and expansion of existing HO lesions *(85)*.

1.2.2.3 Progenitor cell populations

An ongoing goal in the FOP research field has been to identify the progenitor cell populations contributing to the development of heterotopic ossification. Mouse models have been indispensible for progress towards this goal. Several studies have used non-ACVR1-mediated mouse models of HO development, including transgenic BMP4 overexpression *(46, 48, 49, 52)*, Matrigel delivery of BMP2 *(49, 51)*, and BMP2-loaded collagen scaffold delivery coupled with cardiotoxin injection injury *(86)*. Many candidate cell populations were excluded as HO-contributing cells through these experiments, such as FoxD1+ mesenchymal cells *(48)*, CD19+ B-cells, LCK+ T-cells, Lyz+ neutrophils, Myf5+ myoblasts, and nestin+ nerve progenitor cells *(46)*. The studies did identify a

number of contributing progenitor cell populations however, namely Tie2+ endothelial cells *(49, 51)*, COP cells *(52)*, Glast-expressing cells *(48)*, and tendon-derived Scx+ cells *(86)*.

In addition, lineage-tracing studies have been conducted in the constitutively active ACVR1 mouse models to identify progenitor cells contributing to HO. Tie2+ cell contributions to HO lesions were confirmed in both the *Acvr1*^{Q207D} mouse model *(50)* and in the *Acvr1*$^{R206H/+}$ chimeric mouse model *(38)*. Scx+ cells and bone-marrow-derived muscle-resident Mx1+ cells were identified as HO contributing populations in the conditional-on knock-in *Acvr1*^{R206H} mouse model *(47)*.

1.2.3 Embryonic chicken model

After identification of an FOP patient carrying the variant FOP mutation p.Q207E who displayed only classical FOP phenotypes, researchers chose to study the role of this mutation, as well as the classical p.R206H mutation and the engineered p.Q207D mutation, in early limb development *(13)*. All three variants are closely positioned in the GS domain of ACVR1, suggesting that they might cause similar constitutive activation of ACVR1. Overexpression of ACVR1^{R206H} and ACVR1^{Q207E} in chick limbs caused FOP-like phenotypes, including joint fusions and ectopic cartilage formation *(13)*. Overexpression of ACVR1^{Q207D} strongly exacerbated the FOP-like phenotypes, causing severe skeletal malformations and massive ectopic cartilage lesion formation *(13)*. This work provided crucial evidence that the engineered p.Q207D is biochemically distinct from the FOP-associated variants and only marginally appropriate for modeling FOP in animals.

1.2.4 Embryonic zebrafish models

Since its discovery in 1998, zebrafish Acvr1l (previously known as Alk8) has largely been studied for its important role in establishing the dorsoventral axis in the developing embryo *(65, 87-89)*. Expression of kinase-mutated or truncated loss-of-function forms of Acvr1l in the zebrafish embryo result in dorsalization phenotypes, such as loss of ventral tail structures and tail shortening *(87-89)*. Alternatively, embryonic expression of constitutively active Acvr1l, in the form of Acvr1l^{Q204D}, leads to ventralized features that include loss of anterior structures and expansion of ventral mesodermal tissues *(87, 88)*. Both dorsalization and ventralization ultimately result in embryonic death *(87-89)*.

Following the identification of the FOP-associated p.R206H mutation, experiments were conducted in zebrafish embryos to determine whether overexpression of human ACVR1^{R206H} caused developmental defects similar to those of Acvr1l^{Q204D} *(90)*. Indeed, overexpression of human ACVR1^{R206H} resulted in strong ventralization of zebrafish embryos, an effect that required functional downstream BMP/Smad signal transduction, but not BMP2 or BMP7 ligand stimulation *(90)*.

1.2.5 Adult zebrafish model

In this thesis, I describe my work dedicated to creating, validating, and using the first adult zebrafish model for FOP. First, we hypothesized that conditional expression of constitutively active Acvr1l in adult zebrafish would promote the development of FOP-like phenotypes. Given that embryonic expression of both zebrafish Acvr1l^{Q204D} and human ACVR1^{R206H} cause lethality in zebrafish *(87, 88, 90)*, the use of a conditional gene expression system was imperative to establish such a model. Transgenic zebrafish

were created that express heat-shock-inducible Acvr1l^{Q204D} and were exposed to heat-shock to induce Acvr1l^{Q204D} expression at 14 days post fertilization, allowing them to exhibit normal embryonic patterning *(91)*. Chapter 2 describes the generation of these animals and the analysis of their phenotypes after several months of daily heat shock.

Second, we hypothesized that injury of adult heat-shocked Acvr1l^{Q204D}-expressing zebrafish would result in reliable, site-directed HO formation. We used three methods of injury, recombinant human activin A injection, cardiotoxin injection, and caudal fin clip, to assess the development of HO both at the site of injury and globally. Chapter 3 describes these injury experiments, analyses of the phenotypes that developed following injury, and future research directions based on the results.

1.3 Advantages of Adult Zebrafish as a Model for Human FOP

Recent comprehensive natural history studies in human FOP patients have indicated that clinical progression of the disease does not necessarily require a classical flare-up *(16)*. This finding strengthens the need to continue studies of basic developmental pathways of FOP in animal models in order to elucidate all of the molecular pathways mediating, and contributing to, the progression of FOP. Many of these basic research questions can be answered by taking advantage of the tractability of the zebrafish model. Numerous advantages of the zebrafish model system are described below.

1.3.1 Basic biology

Many benefits of the zebrafish as a model for human disease derive from the basic biology of the animal. A pair of adult zebrafish can produce individual clutches of ~200-300 embryos per week, which undergo synchronous, ex utero development and are

optically transparent. These embryos are small enough to fit into 96-well plates, but large enough for manipulations such as microinjection. Embryonic development is rapid and has been extensively studied and documented *(92)*. Zebrafish reach sexual maturity around 3 months post fertilization and many remain fertile for well over a year. Adult zebrafish develop many of the same organs, which function in nearly the same capacity, as other vertebrates, including humans. For example, zebrafish have fully functional, well conserved innate and adaptive immune systems *(93)*, which are crucial in order to study the integral role of the immune response in the early initiation of HO formation in FOP *(85, 94)*.

1.3.2 Genetic manipulation for modifier screens

The fully sequenced zebrafish genome offers evidence for the existence of more than 26,000 protein-coding genes, approximately 70% of which are orthologs of human genes *(95)*. This high degree of conservation at the nucleotide sequence level, when combined with the ease of genetic manipulation by chemical mutagenesis *(96)*, transgenesis *(97)*, and CRISPR/Cas9 editing *(98)*, makes the zebrafish a particularly useful model in which to conduct relatively rapid genetic modifier screens for FOP. Human FOP patients display variability in the rate and severity of disease progression *(4, 99)* and this variability may be caused in part by genetic mutations outside of the ACVR1 locus, which may either suppress or exacerbate aberrant signal activation and alter FOP disease progression. Candidate gene mutations could be easily introduced into the zebrafish genome and assessed for their ability to alter the severity of phenotypes in the zebrafish FOP model.

1.3.3 Reporter lines for lineage tracing

Zebrafish are uniquely amenable to live cell lineage tracing due to their transparency, which can even be maintained in adults through the use of *casper* mutants *(100)*. In addition, there exists a wide variety of currently available fluorescent transgenic reporter lines, including many promoter-driven cell-type specific reporter lines, to study FOP. Finally, a number of conditional gene expression systems have been adapted for use in zebrafish, such as heat-shock induction *(101)*, Cre/*lox* recombination *(102)*, and photoconversion *(103)*. Many, if not most, of these transgenic lines can be easily obtained from the NIH-sponsored Zebrafish International Resource Center (ZIRC), or from individual labs. These resources can be used to validate existing identified progenitor cell populations contributing to human FOP, as well as to identify novel contributing populations using the zebrafish FOP model.

1.3.4 High throughput *in vivo* drug screening

Given their high fecundity and rapid embryonic development, zebrafish are the ideal *in vivo* FOP model system to validate therapeutic compounds identified through in vitro tissue culture assays. In addition, high-throughput screening of novel small molecules and antibodies can be conducted in zebrafish – a benefit exclusive to zebrafish among the existing vertebrate models of human FOP *(104)*. Such compound screens could help identify additional key regulators of HO initiation and progression in FOP, providing new inroads to novel and effective therapies to treat human FOP. Typically, compounds identified through in vivo screens in whole animal models perform better in human clinical trials.

1.4 Conclusions and future directions

The variety of animal models that have been generated for the study of FOP have already been used to provide an incredible wealth of information about the basic mechanisms driving FOP disease progression and potential therapeutic advances. We anticipate that future studies will elucidate the progenitor cell type(s) contributing to HO in FOP patients, and identify new therapeutic targets. Given the variability in FOP disease progression, we also expect that personalized medicine approaches will be designed to more effectively treat individual patients. These therapies may target and regulate multiple mechanisms of BMP signal activation, based on a patient's individual genetic profile. These scientific questions can be quickly and safely probed first in animal models for FOP, to benefit all of the present and future human FOP patients.[1]

[1] This introduction is a modified version of M. LaBonty, P. C. Yelick, Animal models of fibrodysplasia ossificans progressiva, Dev. Dyn. 247, 279–288 (2018). It was adapted with permission of the publisher. Changes include altering the text in section 1.2.5, Adult zebrafish model, to serve as an introduction relevant to the results and conclusions presented in the material that follows.

Chapter 2

A Zebrafish Model of Human Fibrodysplasia Ossificans Progressiva[2]

[2] M. LaBonty, N. Pray, P. C. Yelick, A Zebrafish Model of Human Fibrodysplasia Ossificans Progressiva, *Zebrafish* **14**, 293–304 (2017). Reprinted here with permission of the publisher.

2.1 Introduction

Heterotopic ossification (HO) is a condition in which bone forms outside of the normal skeleton *(6)*. Fibrodysplasia Ossificans Progressiva (FOP), a predominantly sporadic (noninherited) disease that can also be inherited in an autosomal dominant fashion, is characterized by progressive HO *(1-5)*. Initial diagnosis is usually made based on the presence of big toe malformation identifiable at birth, and later in life through the formation of subsequent joint and vertebral fusions, and HO formation within fibrous tissues, including skeletal muscle, ligaments, and tendons *(4)*. Notably, the diaphragm, tongue, and cardiac and smooth muscle are unaffected by FOP *(4)*. FOP patients usually form HO by 7 years of age, experience progressively limited mobility into their teens as the fibrous tissues of their upper body ossify, and are wheel chair bound in their 30's. The median age of survival is 40 years *(4)*. FOP affects ~1 in every 2 million individuals, and is most commonly acquired by spontaneous germline mutation. All individuals with FOP carry activating mutations in the gene encoding ACVR1 (also known as ALK2), with a majority of cases displaying the classic p.R206H mutation *(8, 105)*.

ACVR1 is a member of the Type I TGFβ/BMP receptor family. In TGFβ/BMP signaling, a common mechanism of signal transduction is utilized where an extracellular ligand dimer, including bone morphogenetic proteins (BMPs), activin, inhibin and others, initially binds to a Type II receptor dimer *(24)*. This complex then recruits a Type I receptor dimer, forming a heteromeric complex composed of ligand dimer, Type II receptor dimer, and Type I receptor dimer. Within this complex, the Type II receptors transphosphorylate the Type I receptors in their glycine-serine domains, thereby activating the signaling complex. Activated Type I receptors are then competent to

phosphorylate downstream cytoplasmic Smad signaling partners, which subsequently translocate to the nucleus where they act as transcription factor complexes, in association with other coactivators and corepressors *(24)*. TGFβ/BMP signaling pathways are highly regulated and orchestrate a wide range of cellular processes. In particular, BMP ligands have the unique ability to activate endochondral ossification, a natural pathway for bone formation that is aberrantly activated in HO development in FOP *(39)*.

The first isolation and characterization of *acvr1l/alk8*, the zebrafish ortholog of human *ACVR1*, was conducted in the Yelick lab *(65)*. In addition to strong sequence homology (84% in serine/threonine kinase domain) *(65)*, zebrafish *acvr1l* maps to a chromosomal region of zebrafish linkage group 2 (LG02) that exhibits significant synteny to human *ACVR1* located on human chromosome 2 *(87)*. The *acvr1l* gene is widely expressed during embryonic development and also is expressed maternally *(65, 89)*. Functional characterization of *acvr1l* during early embryonic development in zebrafish revealed critical roles in early dorsoventral patterning. Single cell injections of constitutively active *acvr1l* mRNA produced ventralized embryos that display expanded ventral structures, including ventral tail mesoderm *(87-89)*. In contrast, single cell injections of kinase mutated and dominant negative *acvr1l* mRNA resulted in dorsalized embryos exhibiting loss of ventral tissues and shortened tails *(87, 89)*. Expression of either constitutively active or kinase mutated *acvr1l* results in embryonic lethality by ~3 days post fertilization (dpf) *(87-89)*.

In order to study roles for Acvr1l in later developmental events such as skeletogenesis, we created transgenic zebrafish expressing an mCherry-tagged, heat-shock-inducible copy of Acvr1l containing a Q204D activating mutation, herein called

Acvr1l^{Q204D}. The use of a heat-shock-inducible gene expression system allows us to express Acvr1l^{Q204D} after early embryonic dorsoventral patterning has occurred, to study FOP-like disease progression in zebrafish. We also established an effective, automated heat-shock system, based on a previously published design *(106)*, for both short-term (<1 month) and long-term (>1 month) heat-shock-induced gene expression in juvenile and adult zebrafish. Our experiments using the automated heat-shock system represent the first long-term heat-shock experiments ever used to study an adult zebrafish disease model.

We first demonstrated that heat-shock of transgenic *Tg(acvr1l_Q204D)* embryos at 5 hours post fertilization (hpf) induced ubiquitous expression of Acvr1^{Q204D}, and resulted in ventralized phenotypes, consistent with previous reports *(87-89)*. Expression of mCherry-tagged Acvr1l^{Q204D} was confirmed in heat-shocked adults by fluorescence imaging, Western blot analysis, and Acvr1l immunohistochemical (IHC) analysis. We then characterized the development of FOP-like phenotypes in heat-shocked adult *Tg(acvr1l_Q204D)* zebrafish, which included small HO lesions, abnormal spinal curvature, vertebral fusions, and pelvic fin malformations, suggesting that these animals can be used as a model for human FOP. Here we describe our novel methodology for developing and characterizing a heat-shock inducible adult zebrafish disease model and present our results to date. We describe future studies to enhance the utility of this zebrafish disease model to significantly improve our knowledge and understanding of the cellular and molecular nature of human FOP.

2.2 Materials and Methods

2.2.1 Zebrafish husbandry

Zebrafish (*Danio rerio)* were raised in the Tufts Yelick Lab Zebrafish Facility at 28.5°C in a controlled, automated recirculating environment, with 14/10 hour light/dark cycle, as previously described *(107)*. Zebrafish of both sexes were used in this study, at ages indicated in the manuscript. We used the following mutant and transgenic strains: *Tg(Bre:GFP) (108), Tg(Bre:*GFP*); Tg(hsp70l:acvr1l-mCherry),* and *Tg(Bre:*GFP*); Tg(hsp70l:acvr1l_Q204D-mCherry).*

2.2.2 Ethics statement

All experimental procedures on zebrafish embryos and larvae were approved by the Tufts University Institutional Animal Care and Use Committee (IACUC) and Ethics Committee.

2.2.3 Generation of transgenic animals

Tg(hsp70l:acvr1l-mCherry) and *Tg(hsp70l:acvr1l_Q204D-mCherry)* constructs were generated using the Tol2kit, a gateway-based cloning kit for generating Tol2 transgenesis plasmids *(109)*. In brief, the coding sequence for wildtype (WT) zebrafish Acvr1l or Acvr1l carrying the activating mutation Q204>D (CAG>GAC) were inserted into the multiple cloning site of pME-MCS, generating pME-*acvr1l* or pME-*acvr1l_Q204D*, respectively. Three-part Gateway cloning recombination reactions were used to combine the p5E-*hsp70l* (1.5 kb hsp70l promoter), one of the two pME constructs, and p3E-mCherrypA (mCherry for C-terminal fusions, plus SV40 late polyA). The combined constructs, *hsp70l:acvr1l-mCherry* and *hsp70l:acvr1l_Q204D-mCherry*,

were each inserted into pDestTol2pA2 (an attR4-R3 gate flanked by Tol2 inverted repeats).

*Tg(Bre:*GFP*); Tg(hsp70l:acvr1l-mCherry)* and *Tg(Bre:*GFP*); Tg(hsp70l:acvr1l_Q204D-mCherry)* zebrafish lines were created by single cell injections of the above pDestTol2pA2 constructs and Tol2 transposase mRNA at a final combined concentration of 25 ng/µl in 0.2 M KCl, as previously described *(97)* into homozygous *Tg(Bre:*GFP*)* embryos. Injected animals were raised to adulthood and incrossed to establish stable homozygous transgenic lines for each construct. The following shorthand names are used in this manuscript: *Tg(hsp70l:acvr1l-mCherry)* is referred to as *Tg(acvr1l)*, protein product as Acvr1l^{WT}; *Tg(hsp70l:acvr1l_Q204D-mCherry)* is referred to as *Tg(acvr1l_Q204D)*, protein product as Acvr1l^{Q204D}.

2.2.4 Heat-shock procedures

To validate the expression and function of Acvr1l^{WT} and Acvr1l^{Q204D}, embryonic zebrafish were heat-shocked for 1 hour starting at 5 hpf. In brief, embryos were collected into Eppendorf tubes containing egg water, placed into a beaker of room temperature (RT) water, and then placed into a 38°C water bath for 1 hour. The temperature of the water in the beaker was monitored until it reached 38°C, and heat-shock was allowed to proceed for 1 hour, after which the beaker containing the embryos was moved back to RT. Following recovery at 28.5°C for 19 hours, 24 hpf animals were anaesthetized using 150 mg/L tricaine methanesulfonate (Argent Aquaculture, Redmond, WA, USA) and analyzed for fluorescent reporter transgene expression and phenotypic variations.

A long-term automated heat-shock system for juvenile and adult zebrafish was designed as previously described *(106)*. In brief, submersible heater controller systems

(Pro Heat IC 50W, Won Brothers, Fredericksburg, VA, USA) were calibrated to heat to 38°C, then placed in individual fish tanks. Each heater was plugged into a power strip, which was connected to an outlet timer (TN111, Intermatic, Spring Grove, IL, USA). Starting at 14 dpf, zebrafish were subjected to a once daily 1-hour heat-shock at 38°C. The temperature in each tank was monitored every minute using a four-channel temperature logger with digital display (UX120-006M, Onset Computer, Bourne, MA, USA). At collection time points, animals were lethally anaesthetized using 250 mg/L tricaine methanesulfonate and analyzed for reporter transgene expression and phenotypic variations before micro-computed tomography (Micro-CT) analysis, or further processing for histological and/or IHC analyses.

2.2.5 Fluorescence microscopy

Anaesthetized embryonic and adult *Tg(Bre:GFP)*, *Tg(Bre:GFP); Tg(acvr1l-mCherry),* and *Tg(Bre:GFP); Tg(acvr1l_Q204D-mCherry)* zebrafish were monitored for mCherry fluorescence using a 10.3 s exposure and for GFP using a 4.2 s exposure. All microscope settings were kept constant to allow for comparison of different treatments and transgenic lines. Fluorescence microscopy was conducted using an M2-Bio fluorescent dissecting microscope (Zeiss, Oberkochen, Germany). Images were captured using an Axiocam 503 color camera (Zeiss, Oberkochen, Germany) and processed using AxioVision SE64 microscopy software (Zeiss, Oberkochen, Germany).

2.2.6 Western Blotting

Protein lysates were prepared from age- and size-matched adult zebrafish after three months of continuous heat-shock as follows. Zebrafish were lethally anaesthetized using 250 mg/L tricaine methanesulfonate and then submerged in liquid nitrogen for 5

minutes. Frozen zebrafish were placed in a chilled mortar and homogenized to obtain a fine powder. The dry powder was then transferred to protein extraction buffer (1:10 volume of powder to extraction buffer) *(110)* containing protease inhibitors (cOmplete Protease Inhibitor Cocktail, Roche, Indianapolis, IN, USA) and incubated on ice for 10 minutes. Lysates were clarified by centrifugation at 14,000 *g* for 20 minutes and stored at -20°C until use. Total protein content was quantified using the DC Protein Assay (Bio-Rad, Hercules, CA, USA). Samples (50 ug) were separated by SDS-PAGE using 12% resolving and 6% stacking gels. Proteins were transferred to polyvinylidene fluoride (PVDF) membranes and blocked for 1 hour in 5% milk powder in Tris-buffered saline with Tween-20 (TBST). Membranes were probed overnight at 4°C with the following primary antibodies in 5% milk powder in TBST: Rabbit anti-mCherry at 1:1,000 (ab167453, Abcam, Cambridge, MA, USA), Rabbit anti-GFP at 1:1,000 (ab6556, Abcam, Cambridge, MA, USA), and Mouse anti-β-actin at 1:10,000 (A-5441, Sigma-Aldrich, St. Louis, MO, USA). Membranes were incubated for 1 hour at RT with one of the following peroxidase-conjugated secondary antibodies in 5% milk powder in TBST: Goat anti-rabbit at 1:2,000 (7074, Cell Signaling Technology, Danvers, MA, USA), or Goat anti-mouse at 1:5,000 (31430, Thermo Fisher Scientific, Waltham, MA, USA). Protein bands were detected by chemiluminescence (Pierce ECL Western Blotting Substrate, Thermo Fisher Scientific, Waltham, MA, USA). The size and density of the protein bands were quantified using ImageJ software (https://imagej.nih.gov/ij/).

2.2.7 Histology and immunohistochemistry

Lethally anaesthetized adult zebrafish were fixed in Modified Davidson's Fixative for 48 hours at RT, then rinsed and stored in phosphate-buffered saline (PBS) at 4°C. For

paraffin embedding, samples were immersed for 1 hour each in graded ethanol (25% and 50% in PBS, 75% in water, 100%), followed by xylene immersion overnight. Samples were transferred to molten Paraplast Plus paraffin (McCormick Scientific, St. Louis, MO, USA) and allowed to equilibrate overnight. Samples were embedded in fresh molten paraffin and allowed to solidify at RT. Paraffin blocks were serially sectioned at 7 μm and mounted on SuperFrost Plus charged glass microscope slides (Fisher Scientific, Pittsburgh, PA, USA). For histological analyses, mounted sections were stained with H&E, Safranin O with a Fast Green counter stain, or Hall's and Brunt's Quadruple (HBQ) stain *(111)*. For Safranin O staining, slides were submerged in 0.02% Fast Green in 0.2% acetic acid for 15 seconds followed directly by submersion in 1% Safranin O for 30 seconds. For HBQ staining, samples were stained in the following solutions, in order: Celestine Blue (C7143, Sigma-Aldrich, St. Louis, MO, USA) for 30 seconds; Mayer's Hematoxylin (MHS16, Sigma-Aldrich, St. Louis, MO, USA) for 1 minute; acid alcohol (0.5% glacial acetic acid in 80% ethanol) for 2 minutes; Alcian Blue (05500, Sigma-Aldrich, St. Louis, MO, USA) for 5 minutes; 1% phosphomolybdic acid for 5 minutes; and 0.5% Direct Red (CI 28160, 195251, Sigma-Aldrich, St. Louis, MO, USA) for 4 minutes.

Paraffin sections were also used for IHC analyses. In brief, sections were deparaffinized in xylene and then rehydrated through graded ethanol. Endogenous peroxidases were blocked by treatment with 3% hydrogen peroxide in methanol. Antigen retrieval was completed in a steamer using sodium citrate buffer, pH 6.0. Sections were blocked in 10% serum, incubated with primary antibody in 2% serum for 1 hour at RT, and then incubated with a horseradish peroxidase (HRP)-conjugated secondary antibody

in 2% serum for 45 minutes at RT. Colorimetric signal was developed by incubation of VECTASTAIN Elite ABC reagent (Vector Laboratories, Burlingame, CA, USA), followed by addition of SIGMAFAST DAB reagent (Sigma-Aldrich, St. Louis, MO, USA). Sections were counterstained with Fast Green as already described. After dehydration, slides were mounted using Permount (Fisher Scientific, Pittsburgh, PA, USA) and cover slipped. All stained slides were visualized using a Zeiss AxioPhot epifluorescence microscope (Zeiss, Oberkochen, Germany). Images were captured as described previously.

For IHC analyses, the following antibodies were used: 1:2000 rabbit anti-Acvr1l (custom antibody); and 1:500 donkey anti-rabbit (Jackson ImmunoResearch Laboratories, West Grove, PA, USA).

2.2.8 Micro-computed tomography (Micro-CT)

Euthanized adult zebrafish were imaged using a Skyscan 1176 high-resolution Micro-CT Scanner (Bruker, Allentown, PA, USA). Animals were immersed in a small volume of PBS on a piece of plastic wrap to keep them moist while providing the least background interference during the imaging process. Scans were completed at 9 μm resolution, every 0.5° over 180°. Reconstructions were completed using NRecon (Bruker, Allentown, PA, USA) and 3D volume renderings were generated using CTVox (Bruker, Allentown, PA, USA). All reconstruction and rendering settings were kept constant between samples to allow for comparison.

2.2.9 Alizarin Red Staining

Euthanized adult zebrafish were stained for bone mineralization with Alizarin Red, as previously described with minor modifications *(112)*. In brief, pigment was

cleared in a 1% hydrogen peroxide in 1% potassium hydroxide (KOH) solution for 2 hours. Animals were rinsed in distilled water three times, then transferred to 30% saturated sodium tetraborate (borax) solution overnight. Soft tissues were digested by shaking in 1% trypsin, 2% Borax solution for 6 hours. Animals were rinsed in distilled water three times, then immersed in 10 mg/ml Alizarin Red (A3757, Sigma-Aldrich, St. Louis, MO, USA) in 1% KOH overnight. Animals were rinsed once more in distilled water, then transferred through a glycerol : 1% KOH series (20:80, 40:60, 70:30) over the course of 3 days. Animals were transferred to 100% glycerol for imaging and long-term storage.

2.2.10 Spinal Angle Measurements

The angle of upward (kyphotic) or downward (lordotic) curvature of the spine was measured on a sagittal view of each zebrafish imaged by Micro-CT. Briefly, the angle tool on ImageJ was used to place three points: the first at the peak of the curvature of the spine, the second at the Weberian apparatus anterior to the vertebrae, and the third at the hypural joint posterior to the vertebrae. The angle created by these three points was measured and recorded as the spinal angle, in degrees. Positive numbers indicate kyphosis, which is the natural curvature for anterior vertebrae *(113)*, while negative numbers indicate lordosis, which is abnormal spinal curvature in a zebrafish.

2.2.11 Methodology and Statistics

All animals established on a given heat-shock system were included in analyses described hereunder. Animal numbers and replicates are indicated in figure legends. Only animals that died of natural causes prior to desired collection time point were excluded

from analyses. Spinal angle measurements were compared with an unpaired *t*-test using GraphPad Prism statistical software.

2.3 Results

2.3.1 Generation of *Tg(acvr1l_Q204D)* zebrafish for conditional expression of constitutively active Acvr1l

Before the identification of constitutively activating mutations in *ACVR1* as the underlying cause of FOP in humans *(7)*, the zebrafish homolog of human *ACVR1*, presently known as *acvr1l* and previously known as *alk8*, was studied for its role in early embryonic development and dorsoventral patterning *(65, 87-89, 114)*. Expression of constitutively active Acvr1l in zebrafish embryos causes ventralization phenotypes, resulting in reduced dorsal neural tissue formation and expanded ventral mesodermal tissue formation *(87-89)*. These strong phenotypes resulted in early embryonic lethality, prohibiting studies of constitutively active Acvr1l in adult zebrafish development.

Therefore, in order to study the effects of constitutively activated Acvr1l expression in juvenile and adult zebrafish, we turned to a conditional gene expression system. We used gateway-based cloning to generate constructs containing the coding sequence for WT zebrafish Acvr1l and the Yelick Lab-generated constitutively active Acvr1 (Q204D) mutant (Figure 2.1A, B), each driven by the Hsp70 promoter. In addition, each construct contained a C-terminal in frame mCherry sequence tag in order to generate a fluorescent Acvr1l-mCherry fusion protein product (Figure 2.1C). These constructs were injected into single-cell stage zebrafish embryos along with Tol2 transposase to promote transgene integration. Stable transgenic lines were established for *Tg(hsp70l:acvr1l-mCherry)*, called *Tg(acvr1l)*, and *Tg(hsp70l:acvr1l_Q204D-mCherry)*,

called *Tg(acvr1l_Q204D)*, which only express the transgenes when exposed to 38°C, and thus exhibit normal embryonic development and patterning when raised at 28.5°C. We injected each of the heat-shock constructs into the transgenic *Tg(Bre:GFP)* zebrafish line, which carries a reporter construct containing five tandem BMP response elements driving GFP expression *(108)*. This reporter line allows us to directly assess the level of activation of BMP signaling in *Tg(acvr1l)* or *Tg(acvr1l_Q204D)* transgenic zebrafish using GFP fluorescent microscopy.

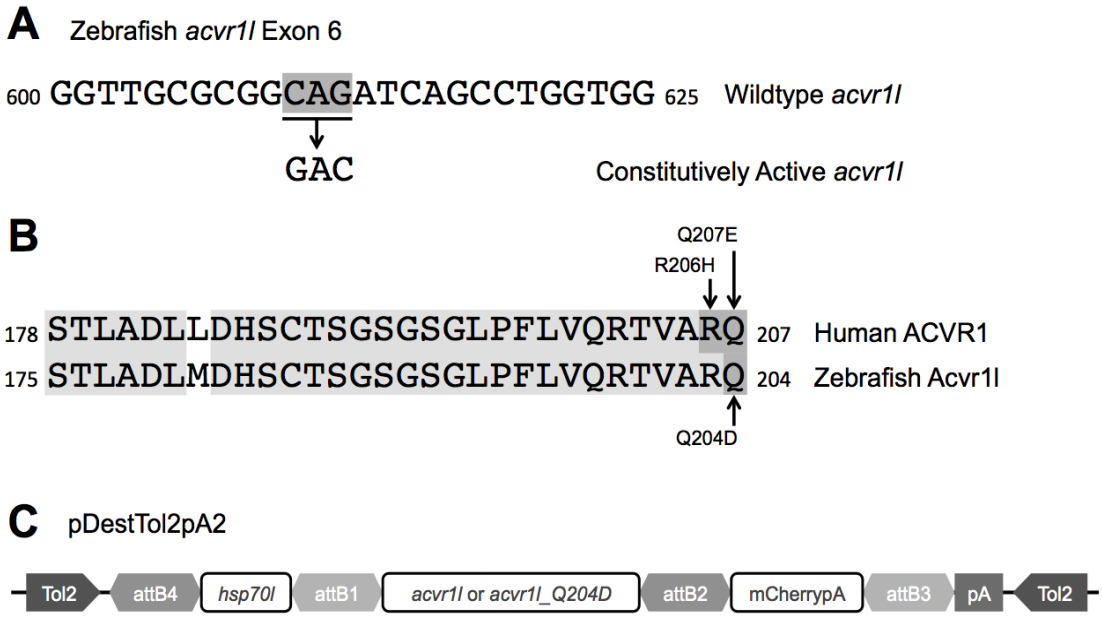

Figure 2.1. Generation of *Tg(Bre:GFP); Tg(acvr1l_Q204D-mCherry)* animals. A Yelick laboratory-created construct for constitutively active zebrafish *acvr1l* contains 2 bp mutations converting a CAG to GAC in exon 4 (A). These mutations result in an amino acid change of glutamine (Q) 204 to aspartic acid (D) in the GS domain of the zebrafish Acvr1l protein (B). Zebrafish Acvr1l p.Q204D is homologous to human ACVR1 p.Q207D, which is one of the variants (along with p.R206H) in the GS domain commonly mutated in FOP patients. (C) Schematic of pDestTol2pA2 constructs to generate *Tg(hsp70l:acvr1l-mCherry)* and *Tg(hsp70l:acvr1l_Q204D-mCherry)*

2.3.2 Automated heat-shock system delivers reliable short-term and long-term heat-shock

Heat-shock induction of gene expression is a well-established method in zebrafish for studying the spatial and temporal roles of proteins *in vivo (101)*. However, few studies have applied heat-shock technology for long-term (>1 month) expression studies in juvenile and adult zebrafish and none have used this technology to generate adult zebrafish disease models. Recently, an economical heat-shock system was established that can be added to any existing recirculating zebrafish rack, and which allows for automation of the heat-shock temperature, duration, and frequency *(106)*. We have outfitted our zebrafish facility with three independent heat-shock systems (Figure 2.2A), each of which is equipped with a temperature logger that registers the temperature in each of up to four tanks, every minute (Figure 2.2B). The data from the temperature loggers can be downloaded to a laboratory computer and graphed to display heat-shock regimens over time (Figure 2.2C).

When establishing our FOP zebrafish heat-shock model, we found the greatest long-term survival using zebrafish that were at least 14 dpf at the start of a heat-shock experiment. We found that daily heat-shock of animals at 7 dpf resulted in the loss of greater than 50% of animals by 14 dpf. Consistent with previous findings *(106)*, we found that a low flow rate of 10-20 mL/min was ideal for reaching and maintaining peak heat-shock temperatures. We determined by fluorescence imaging (mCherry) that once daily heat-shock for 1 hour is sufficient to induce and maintain continuous Acvr1l^{WT} or Acvr1l^{Q207D}-mCherry protein expression. To date, we have used our heat-shock systems

to effectively run experiments ranging in duration from 1 week to 1 year of daily heat-shock on a single cohort of animals.

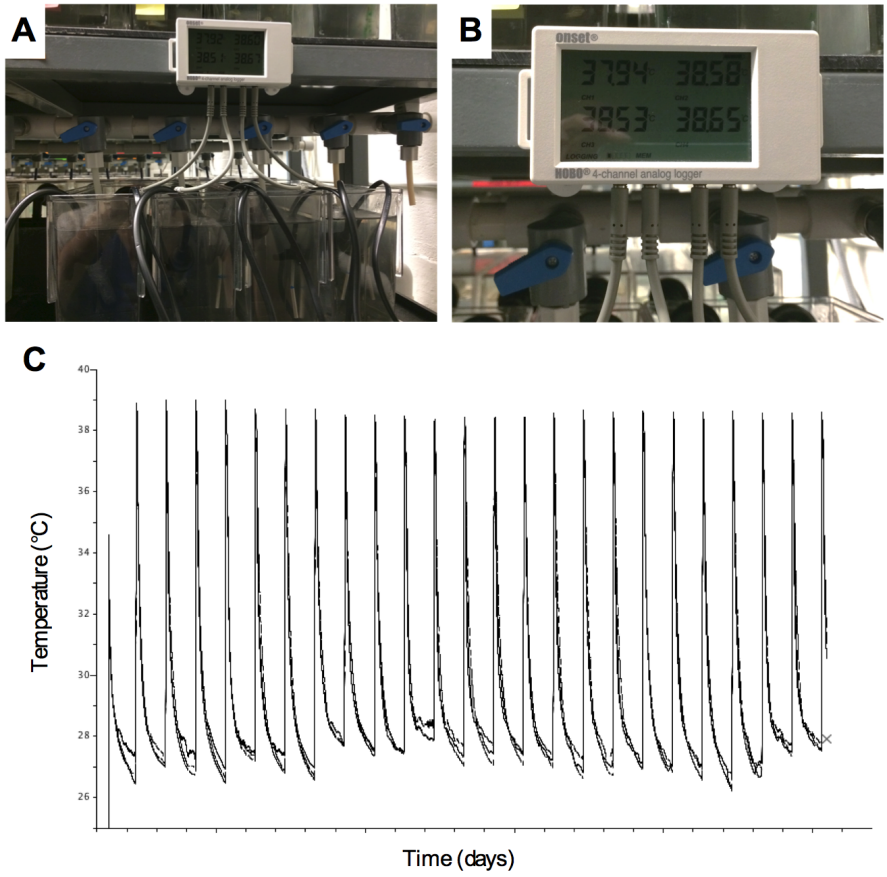

Figure 2.2. Establishment of automated heat-shock system for long-term experiments. Automated heat-shock systems established by installing individual tank heaters in system tanks (A). Heaters were calibrated to perform a once daily 1-hour heat-shock at 38°C, which was monitored every minute of every day by a temperature logger (B, C).

2.3.3 Functional heat-shock *Tg(acvr1l_Q204D-mCherry)* constructs are expressed in embryonic and adult stage zebrafish

To confirm the expression of Acvr1l^{Q207D}–mCherry in the *Tg(Bre:GFP)* reporter background, we first examined expression in embryonic zebrafish. In brief, 5 hpf embryos were treated with 1 hour of heat-shock, and then were analyzed under fluorescent microscopy for mCherry and GFP expression, and using bright field microscopy to confirm the previously characterized ventralized phenotype caused by upregulated BMP signaling *(87-89)*. Heat-shocked *Tg(Bre:GFP)* zebrafish exhibited GFP expression in tissues where BMP signaling is normally active at 24 hpf, including the eye and the somites (Figure 2.3C) *(108)*, but exhibited no mCherry expression at 24 hpf (only yolk autofluorescence is visible) (Figure 2.3B). Dorsoventral patterning appeared normal in *Tg(Bre:GFP)* expressing animals (Figure 2.3A). Heat-shocked zebrafish carrying both *Tg(Bre:GFP)* and *Tg(acvr1l-mCherry)* transgenes also exhibited normal dorsoventral patterning (Figure 2.3D) and displayed normal GFP expression patterns (Figure 2.3F). mCherry was ubiquitously expressed in these animals, as expected for an *hsp70l*-induced transgene (Figure 2.3E). The expression of Acvr1l^{WT}-mCherry following heat-shock did not confer any phenotypic abnormalities and animals proceeded through embryonic development normally, as previously reported *(87)*. In contrast, heat-shocked zebrafish expressing *Tg(acvr1l_Q204D-mCherry)* in the *Tg(Bre:GFP)* background exhibited consistent ventralized phenotypes (Figure 2.3G). mCherry fluorescence was ubiquitous in these animals indicating widespread expression of Acvr1l^{Q204D} (Figure 2.3H), and upregulated GFP expression was observed in nearly all tissues of these animals (Figure 2.3I), indicative of upregulated BMP signaling *(115, 116)*.

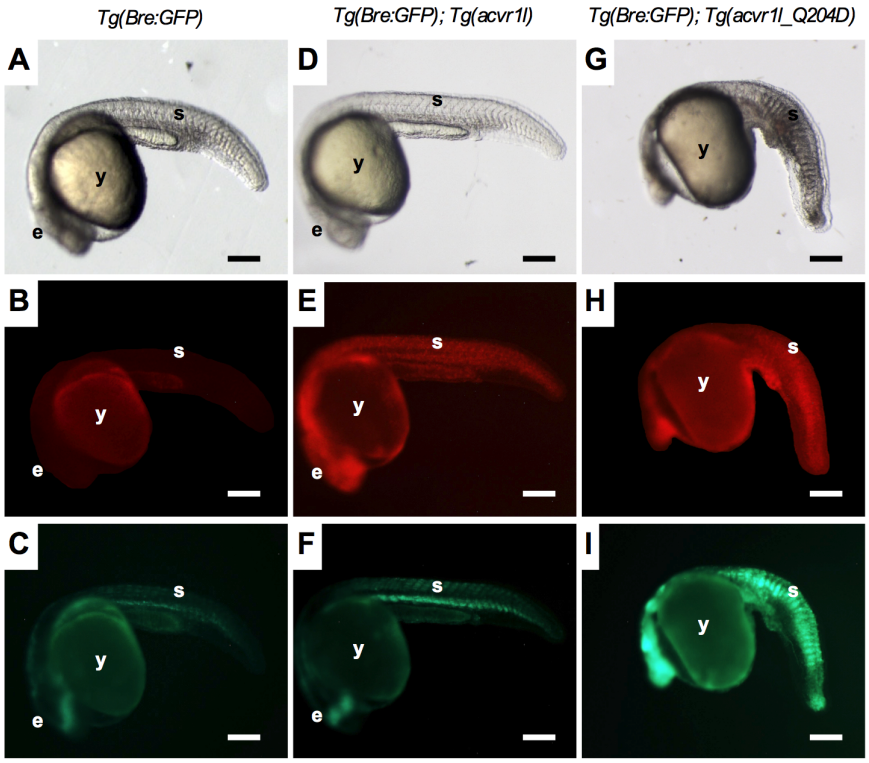

Figure 2.3. *Tg(Bre:GFP); Tg(acvr1l_Q204D-mCherry)* embryos exhibit ventralized phenotypes and increased *Tg(Bre:GFP)* reporter expression. *Tg(Bre:GFP)* (A–C), *Tg(Bre:GFP); Tg(acvr1l-mCherry)* (D–F), and *Tg(Bre:GFP); Tg(acvr1l_Q204D-mCherry)* (G–I) embryos at 24 hpf, after 1 hour of heat-shock at 5 hpf. Embryos were analyzed through fluorescent microscopy for mCherry (B, E, H) and GFP (C, F, I) fluorescence intensity, and through bright field microscopy for gross morphological phenotypes (A, D, G). n = 10 embryos each, for at least three replicate experiments. Scale bar is 200 µm. e, eye, s, somites, y, yolk.

Once confirmed in the embryo, we next investigated functional expression of Acvr1l^{Q204D}-mCherry in adult zebrafish, using fluorescence imaging, western blotting, and IHC analysis of transgenic animals after 3 months of daily heat-shock (Figures 2.4 and 2.5). At 3 months, adult heat-shocked *Tg(Bre:GFP)* zebrafish exhibited GFP expression most prominently in the lens of the eye; although ubiquitous GFP expression throughout the body was detectable anywhere pigment was absent (Figure 2.4C). mCherry expression was not detected in these animals (Figure 2.4B). In contrast, adult heat-shocked *Tg(Bre:GFP); Tg(acvr1l_Q204D-mCherry)* zebrafish exhibited mCherry expression throughout the animal, including very bright expression in the lens of the eye (Figure 2.4E). These animals also exhibited ubiquitous GFP expression; however, this expression did not appear significantly brighter than heat-shocked *Tg(Bre:GFP)* adults (Figure 2.4F), suggesting that visual quantification of GFP fluorescence in live adult zebrafish is likely obscured by the size, scales and pigmentation of adult zebrafish. Therefore, to confirm that heat-shocked adult *Tg(Bre:GFP); Tg(acvr1l_Q204D-mCherry)* zebrafish exhibited upregulated BMP signaling in response to the expression of Acvr1l^{Q204D}, we used Western blotting to quantify mCherry and GFP protein levels in whole animal protein lysates (Figure 2.4G). These analyses showed that only *Tg(Bre:GFP); Tg(acvr1l_Q204D-mCherry)* zebrafish expressed mCherry, with a band at 84 kDa indicative of the Acvr1l-mCherry fusion protein, as expected. We also observed a second band at 27 kDa indicative of free mCherry, suggesting some level of instability and cleavage of the Acvr1l-mCherry fusion protein. We found that heat-shocked *Tg(Bre:GFP); Tg(acvr1l_Q204D-mCherry)* zebrafish exhibited a 3.2-fold increase in GFP protein expression as compared to heat-shocked *Tg(Bre:GFP)* zebrafish, indicative

of upregulated BMP signaling in animals expressing constitutively active Acvr1l. Together, these results demonstrate that heat-shock induced Acvr1l^{Q204D}-mCherry is functional in adult and embryonic zebrafish, and is capable of inducing upregulated BMP signaling measured by increased GFP protein expression.

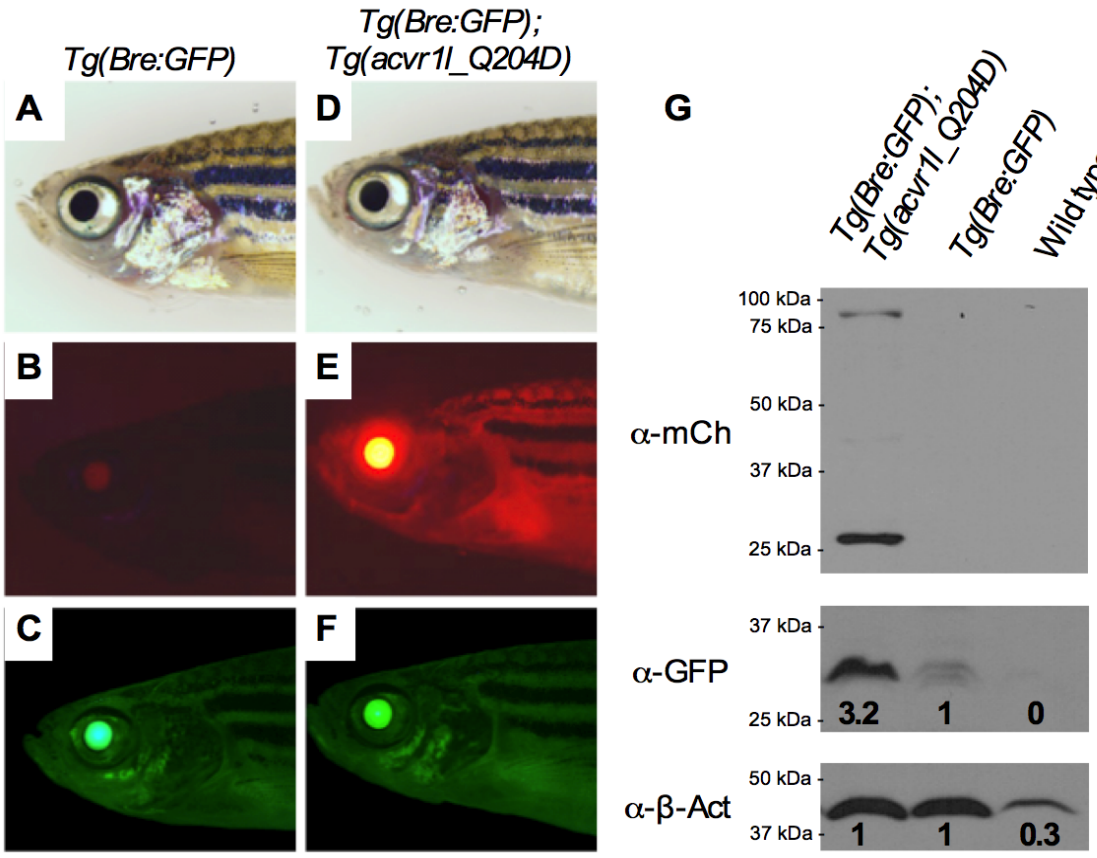

Figure 2.4. Acvr1l^{Q204D} is expressed in heat-shocked adult zebrafish. After 3 months of once daily heat-shock for 1 hour at 38°C, adult *Tg(Bre:GFP)* (A–C) and *Tg(Bre:GFP); Tg(acvr1l_Q204D-mCherry)* (D–F) zebrafish were characterized through bright field microscopy (A, D) and through fluorescent microscopy for mCherry (B, E) and GFP (C, F) fluorescence intensity (n = 5 adult zebrafish). (G) Western blots of protein extracts from the same animals were probed using anti-mCherry (Acvr1l-mCherry at 84 kDa and free mCherry at 27 kDa), anti-GFP (27 kDa), and anti-β-Actin (43 kDa) antibodies (n = 2 replicate western blots).

In addition to validating heat-shock induced Acvr1l^{Q204D}-mCherry expression by fluorescence imaging and Western blotting, Acvr1l^{Q204D}-mCherry expression was also validated using paraffin section IHC for Acvr1l (Figure 2.5). Endogenous levels of Acvr1l were detected in heat-shocked *Tg(Bre:GFP)* zebrafish in most tissues, including the intestines (Figure 2.5B) and the muscle tissue (Figure 2.5E, H); however it was absent from the liver (Figure 2.5B). Upregulated and ubiquitous Acvr1l expression was detected in heat-shocked *Tg(Bre:GFP); Tg(acvr1l_Q204D)* zebrafish, as seen in the intestines, liver, and muscle tissue (Figure 2.5C, F, I), consistent with expression of both endogenous Acvr1l and heat-shock induced Acvr1l^{Q204D} proteins. Previous work from the Yelick lab has demonstrated Acvr1l receptor specificity for this antibody *(117)*. No Acvr1l expression was detected in samples lacking the primary antibody (Figure 2.5A, D, G). Together, our fluorescence imaging, Western blot, and IHC results confirmed the expression of functionally active Acvr1l^{Q204D} in both embryonic and adult heat-shocked zebrafish.

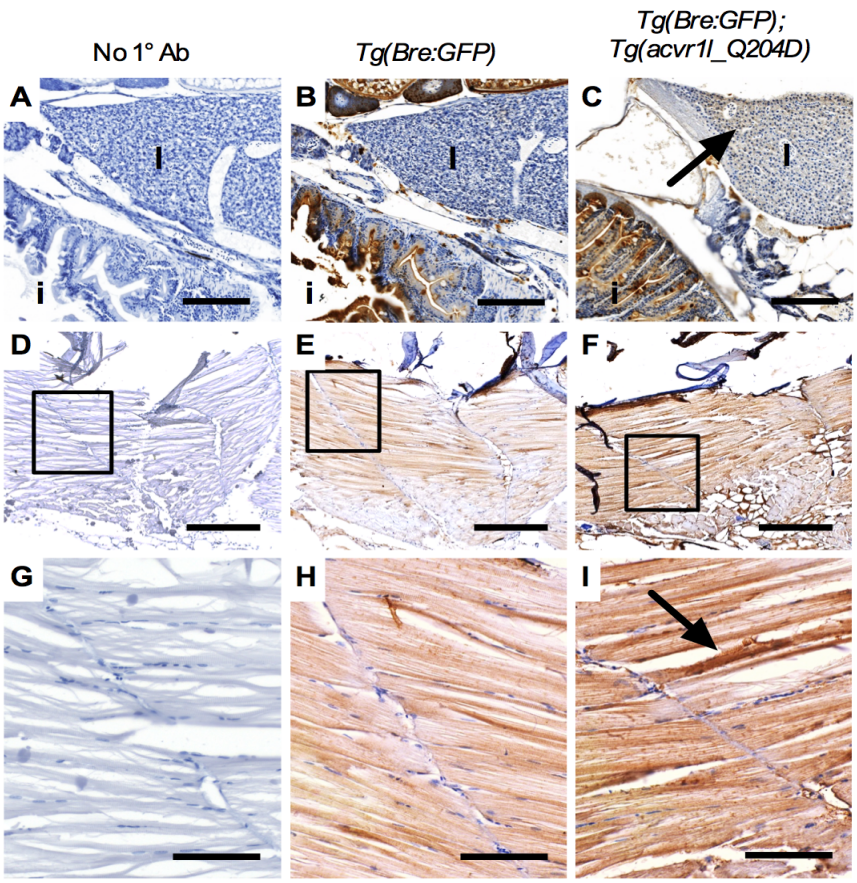

Figure 2.5. Acvr1l^{Q204D} protein expression is ubiquitous. Sagittal paraffin sections of imaged adult *Tg(Bre:GFP)* (B: 20x, E: 10x, H: 40x) and *Tg(Bre:GFP); Tg(acvr1l_Q204D-mCherry)* (C: 20x, F: 10x, I: 40x) zebrafish were used to analyze Acvr1l expression by IHC. No primary controls were negative (A: 20x, D: 10x, G: 40x). Arrows point to regions of greater Acvr1l expression in *Tg(Bre:GFP); Tg(acvr1l_Q204D-mCherry)* zebrafish (C, I). (G–H) are enlarged views of areas indicated by boxes in (D–F). (A–C) 20x scale bar is 150 µm. (D–F) 10x scale bar is 400 µm. (G–I) 40x scale bar is 80 µm. i, intestines, l, liver.

2.3.4 Micro-CT analyses of heat-shocked *Tg(acvr1l_Q204D)* zebrafish reveal phenotypes indicative of FOP

After verifying functional expression of Acvr1l^{Q204D} in heat-shocked adult zebrafish, we next sought to determine whether FOP-like phenotypes were evident in these animals. *Tg(Bre:GFP); Tg(acvr1l_Q204D-mCherry)* zebrafish were heat-shocked daily for 3 to 8 months before euthanization and imaging with Micro-CT (Table 2.1, Figure 2.6). All of the eight heat-shocked *Tg(Bre:GFP); Tg(acvr1l_Q204D-mCherry)* zebrafish examined displayed some degree of spinal lordosis (Figure 2.6B, C), in distinct contrast to the slightly kyphotic spinal curvature exhibited by age-matched non-heat-shocked and heat-shocked *Tg(Bre:GFP)* zebrafish (Figure 2.6A). The average angle of spinal curvature in the *Tg(Bre:GFP); Tg(acvr1l_Q204D-mCherry)* zebrafish was -3.27°, indicative of downward or lordotic curvature (Figure 2.6D). This angle was statistically significantly different from the average angle of the *Tg(Bre:GFP)* zebrafish, 7.74°. Thoracic lordosis is a known developmental phenotype of FOP patients *(4)*.

In addition to the fully penetrant lordosis phenotype observed in heat-shocked *Tg(Bre:GFP); Tg(acvr1l_Q204D-mCherry)* zebrafish, several other FOP phenotypes were observed in some animals. Significantly, 3/8 animals (37.5%) developed small HO lesions just behind the dorsal fin (Figure 2.6H, arrow), and 1/8 animals (12.5%) exhibited significant HO throughout the body cavity (Figure 2.6F, arrow). None of the heat-shocked *Tg(Bre:GFP)* zebrafish developed HO within the body cavity (Figure 2.6E, G). As previously described, HO is one of the hallmark characteristics of human FOP patients *(2, 8)*. Furthermore, we found 3/8 animals (37.5%) displayed single vertebral fusions (Figure 2.6J, arrow), which were never observed in heat-shocked *Tg(Bre:GFP)*

control animals (Figure 2.6I). Vertebral fusions are a common variable phenotype of human FOP *(4)*. In addition, 1/8 heat-shocked *Tg(Bre:GFP); Tg(acvr1l_Q204D-mCherry)* animals (12.5%) showed a strong malformation of both pelvic fins (Figure 2.6L, N, arrows), easily identified as compared to control *Tg(Bre:GFP)* zebrafish (Figure 2.6K, M). Recent work has provided strong support for common developmental pathways driving fish fin ray formation and tetrapod digit formation *(118)*, suggesting that this partially penetrant phenotype could be reminiscent of the big toe malformation associated with classical human FOP, despite being more severe than the human phenotype *(4, 8)*.

	3 months HS			8 months HS					Totals
	Fish 1 (Male)	Fish 2 (Female)	Fish 3 (Male)	Fish 4 (Female)	Fish 5 (Male)	Fish 6 (Female)	Fish 7 (Male)	Fish 8 (Male)	
Lordosis	Yes	Yes	Yes	Yes	Yes	Yes	Yes	Yes	8/8 100%
Vertebral fusion	No	Yes	No	No	Yes	No	No	Yes	3/8 37.5%
HO lesions	No	No	No	No	No	Yes	Yes	Yes	3/8 37.5%
Malformed pelvic fins	Yes	No	No	No	No	No	No	No	1/8 12.5%

Table 2.1. FOP-like phenotypes in *Tg(acvr1l_Q204D-mCherry)* zebrafish. *Tg(Bre:GFP); Tg(acvr1l_Q204D-mCherry)* animals analyzed by Micro-CT after 3 or 8 months of heat-shock displayed various FOP-like phenotypes.

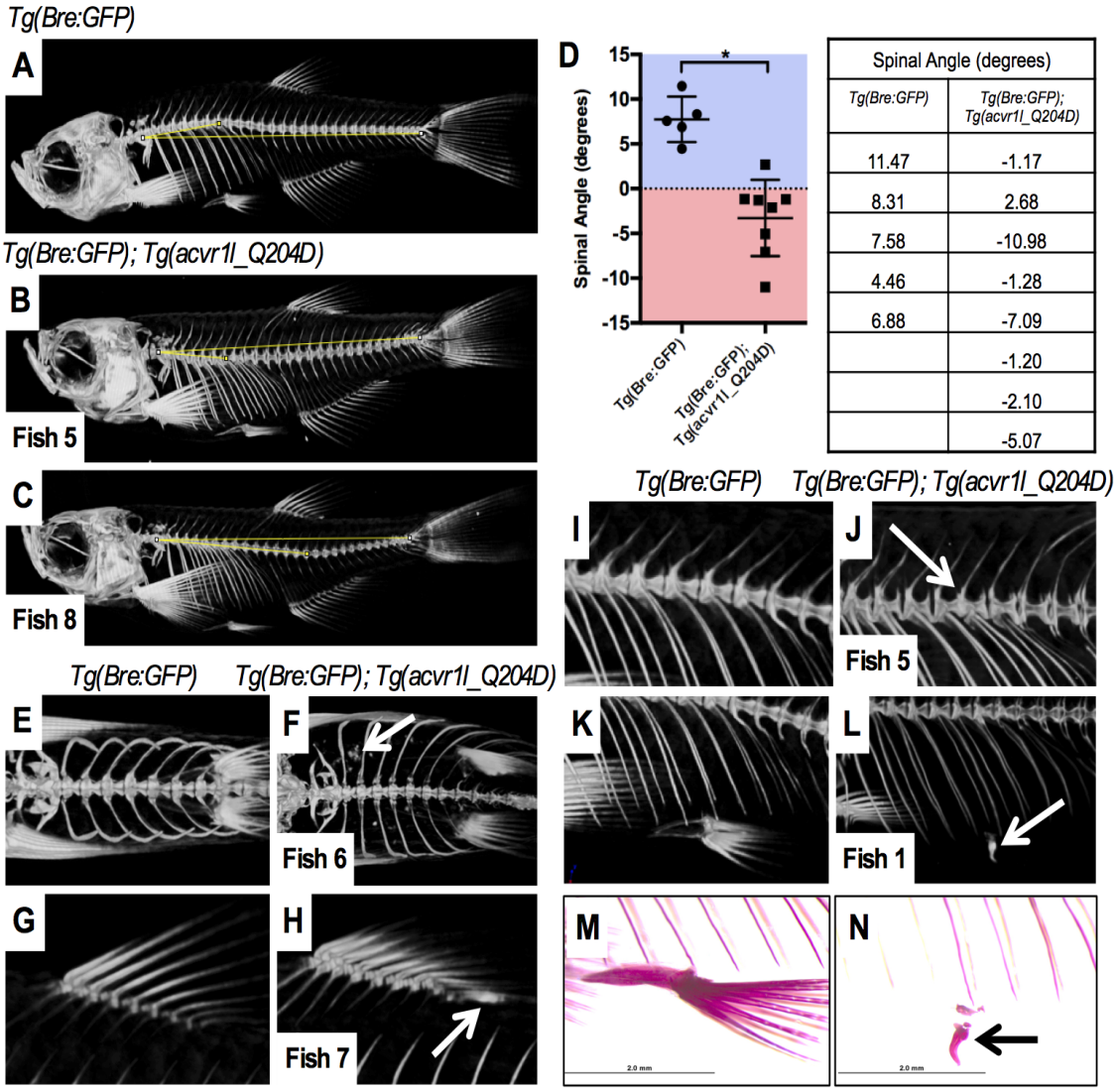

Figure 2.6. Expression of Acvr1l^{Q204D} in zebrafish generates FOP-like phenotypes. Micro-CT imaging of zebrafish expressing Acvr1l^{Q204D}–mCherry revealed a variety of FOP-like phenotypes, including spinal lordosis (B, C, quantified in D) as compared with age-matched *Tg(Bre:GFP)* animals (A); HO (F, H, arrows vs. E, G); vertebral fusion (J, arrow vs. I); and malformed pelvic fins (L, arrow vs. K). Alizarin Red staining of zebrafish harboring malformed pelvic fins indicated abnormal mineralization of structures (N, arrow). Control *Tg(Bre:GFP)* zebrafish did not exhibit any of these phenotypes (A, E, G, I, K, M). Panels containing zebrafish expressing Acvr1l^{Q204D}–mCherry labeled with fish number corresponding to Table 1. n = 8 *Tg(Bre:GFP); Tg(acvr1l_Q204D-mCherry)* animals, and n=5 *Tg(Bre:GFP)* animals. *Indicates statistical significance of P<0.001.

2.3.5 Histological analyses of HO from FOP zebrafish

After successfully identifying HO in heat-shocked *Tg(Bre:GFP); Tg(acvr1l_Q204D)* zebrafish by Micro-CT, these lesions were analyzed at the cellular level using histological analyses including H&E, Safranin O, and HBQ stains *(111)*. H&E-stained sagittal sections of the heat-shocked *Tg(Bre:GFP); Tg(acvr1l_Q204D)* zebrafish exhibiting HO lesions throughout the body cavity (Table 2.1, Fish 6; Figure 2.6F) revealed numerous mineralized tissue-like masses (Figure 2.7A box, D arrow). Safranin O-stained serial sections revealed dark red staining indicative of cartilaginous proteoglycans (Figure 2.7B box, E arrow). HBQ-stained serial sections exhibited pink staining indicative of mineralized tissue formation (Figure 2.7C box, F arrow). Positive staining for both cartilaginous proteoglycans and mineralization is a common feature of human HO lesions *(38, 119)*.

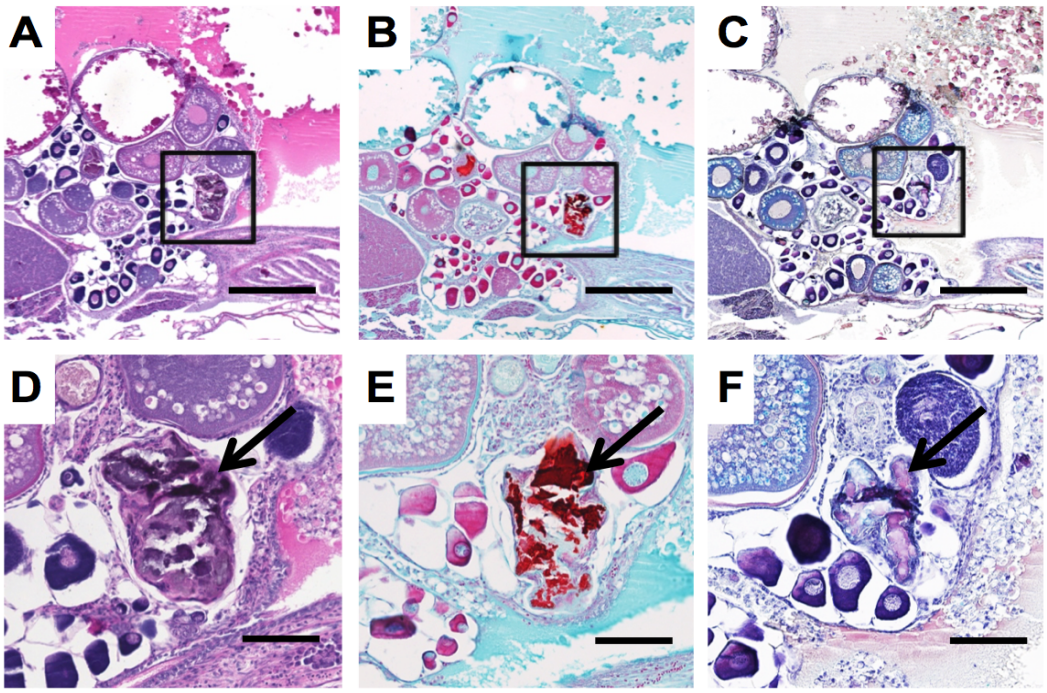

Figure 2.7. Histology of HO in *Tg(acvr1l_Q204D-mCherry)* zebrafish. H&E (A, D), Safranin O (B, E), and HBQ (C, F)-stained paraffin sectioned *Tg(Bre:GFP); Tg(acvr1l_Q204D-mCherry)* zebrafish (A–F). Sagittal sections of zebrafish exhibiting HO throughout the body cavity revealed numerous proteoglycan-dense (B, E, strong red Safranin O stain), ossified (C, F, pinkish-red from HBQ stain) masses adjacent to the ovary (boxed in panels A–C, arrows in panels D–F). (D–F) are enlarged views of areas indicated by boxes in (A–C), respectively. (A–C) 5x scale bar is 400 μm. (D–F) 20x scale bar is 100 um.

2.4 Discussion

In this study, we describe the creation and characterization of the first heat-shock inducible adult zebrafish disease model. Adult zebrafish expressing heat-shock-inducible *Tg(acvr1l_Q204D)*, a transgene encoding a constitutively active form of the zebrafish ortholog of the FOP-associated human gene *ACVR1,* developed a variety of FOP-like phenotypes, including HO, fused vertebrae, pelvic fin malformations, and abnormal spinal lordosis. The significant HO that developed in a heat-shocked *Tg(acvr1l_Q204D)*

zebrafish strongly resembled that observed in human FOP patients, and in an FOP mouse model that was characterized using Micro-CT and histological analyses *(12, 18, 34, 38)*. Although the activating mutation p.Q204D used in these experiments does not naturally occur in human FOP patients, the development of phenotypes associated with FOP suggests that heat-shock-inducible *Tg(acvr1l_Q204D)* zebrafish can still serve as a useful model for studying human FOP.

The variability of penetrance of the phenotypes observed in the heat-shock-inducible *Tg(acvr1l_Q204D)* zebrafish is reminiscent of the variability in the severity of FOP in humans *(4)*. Only two features of the disease in humans are considered to be fully penetrant and classical hallmarks of the disease: malformation of the big toes and progressive HO formation *(2)*. Even the rates of HO formation can vary greatly between human patients, with some individuals immobilized by their HO growth by 20 years of age, whereas others remain nearly unaffected in the same time frame. Most other phenotypes associated with FOP are atypical and variable. For example, osteochondromas develop in >90% of patients, cervical spine malformations affect >80% of patients, and thumb malformations affect ~50% of patients *(8)*. In addition, some FOP patients present with rare, previously undocumented phenotypes, including loss of digits, growth retardation, aplastic anemia, cataracts, and retinal detachment, to name a few *(8)*. This wide range of variability in the development of human FOP phenotypes suggests that the variability seen in the first adult zebrafish model for FOP is to be expected.

These results are particularly exciting due to the numerous advantages afforded by modeling FOP in the zebrafish. First, genetic modifier screens for FOP can be most easily conducted in zebrafish. In human patients with FOP, there is great variability in the

severity of phenotypes and in the rate of disease progression *(4)*. It is likely that this variability is caused in part by additional uncharacterized genetic mutations that synergize with constitutively active Acvr1 to either suppress or exacerbate disease progression. Such mutations could be efficiently identified in a zebrafish model for FOP using well-established tools for mutagenesis, such as chemical N-ethyl-nitroso-urea (ENU) *(96)*, and screening mutagenized animals for alterations in characterized phenotypes. Second, zebrafish are an ideal model system to quickly validate existing therapeutic compounds identified through *in vitro* cell-based assays. In addition, small molecule screens are readily performed in zebrafish as compared with rodent models, and can be used to identify novel signaling pathways that can potentially be exploited as new therapeutic inroads to treat human FOP. *In vivo* drug screens in animals typically provide superior candidates to *in vitro* cell-based assays and also provide insight into the pharmacological properties of drugs, such as metabolism and toxicity. Of all the model organisms amenable to drug screens - yeast, worms, flies, and zebrafish - only zebrafish possess organ systems with well-conserved physiology to human organs *(104)*. Third, zebrafish have fully functional innate and adaptive immune systems which are similar to human immune systems *(93)*. Functional conservation of these systems is critical, as recent research suggests an integral role for immunological triggers in the progression of FOP *(94)*.

The majority of heat-shocked *Tg(acvr1l_Q204D)* zebrafish did not spontaneously develop large HO lesions, as was expected. In retrospect, this may not be entirely surprising, due to the fact that in humans, FOP lesion formation is initiated by accidental injuries, which rarely, if ever, occur in a zebrafish facility laboratory setting. Indeed, lack

of spontaneous HO formation has been observed in other FOP animal models *(46)*. In numerous published animal model FOP studies, an injury model was used to induce HO *(18, 34, 38, 46, 55, 120)*. Advantages that could be afforded by introducing an injury model for FOP zebrafish include reproducibility, easy identification of targeted lesion site, and the potential to perform time course analyses of disease progression. Given these findings, we intend to further our studies by incorporating the future design and implementation of an injury model for our heat-shocked *Tg(acvr1l_Q204D)* FOP zebrafish.

In addition to establishing an injury model for heat-shock-inducible *Tg(acvr1l_Q204D)* FOP zebrafish, future studies will use gene editing techniques such as CRISPR-Cas9 to introduce human FOP-associated mutations at the endogenous zebrafish *acvr1l* locus. Two common FOP-associated mutations in human *ACVR1* are p.R206H (p.R203H in zebrafish) and p.Q207E (p.Q204E in zebrafish) (Figure 2.1B) *(8, 13, 105)*. It has yet to be determined whether heterozygous expression of constitutively active zebrafish *acvr1l* under the control of its endogenous promoter will cause embryonic lethality due to ventralization phenotypes, or whether these animals will successfully undergo embryonic development and subsequently acquire FOP-like phenotypes, as observed in human FOP patients. These approaches may provide a more robust zebrafish model of FOP with which to address further questions in the field.

In summary, this study introduces the first zebrafish model resembling human FOP. Given the conservation of organ system development and physiology between humans and zebrafish, this model provides a new and valuable *in vivo* tool for studying FOP. Future studies will exploit the advantages of the zebrafish model to fill gaps in our

knowledge and understanding of the genetic and molecular mechanisms driving FOP disease progression.

Chapter 3

Injury of adult zebrafish expressing Acvr1l^{Q204D} does not result in heterotopic ossification[3]

[3] M. LaBonty, N. Pray, P. C. Yelick, Injury of adult zebrafish expressing Acvr1l^{Q204D} does not result in heterotopic ossification, To be submitted to *Zebrafish* (2018).

3.1 Introduction

Fibrodysplasia ossificans progressiva (FOP) is a rare human disease, affecting only 1 in 2 million individuals, that is characterized by the presence of big toe malformations and the progressive development of heterotopic ossification (HO) within skeletal muscle, tendons, and ligaments *(1-5)*. While patients are born with malformed big toes, the formation of HO, or FOP lesions, is typically delayed until 5-7 years of age. As the disease progresses, patients experience a progressive loss of mobility due to the ossification of joints and limbs. The cumulative build up of HO in FOP patients results in a decreased average lifespan of 40 years *(4)*. FOP results from spontaneous germline mutations that cause constitutive activation of the Type I TGFβ/BMP receptor family member ACVR1 *(8)*.

The normal progression of an FOP lesion is currently thought to follow a two-phase process *(39)*. In the first phase, inflammation results from a triggering event, which can include a physical injury, a surgical procedure, or a systemic infection *(4, 40, 41)*. Inflammatory cells overwhelm the lesion site and promote muscle tissue degradation, angiogenesis, and fibroproliferation *(42-44)*. In the second phase, a recruited population of mesenchymal stem cells undergoes the process of normal endochondral ossification to generate HO at the site of the FOP lesion *(39)*.

Given that immunosuppression can halt the development of HO in human FOP patients *(45)*, it appears that the immune response resulting from injury may play a critical role in driving the early stages of FOP lesion formation. Thus, an understanding of what cues are promoting an inflammatory response may help in developing therapeutic strategies to mitigate or even abolish the formation of FOP lesions. To this end,

researchers have developed a number of injury models to induce the formation of HO in a consistent site-directed manner *(18, 34, 38, 46, 47, 55, 86, 121-123)*. We have gained a wealth of knowledge about FOP lesion progression from the work that has been done with FOP injury models, including the identification of an abnormal mechanism of activation of ACVR1^{R206H} by activin A *(18, 34)*, progenitor cell populations that make up the mesenchymal stem cell pool *(46, 47, 86)*, an enhancement of mTOR signaling that promotes endochondral ossification *(121)*, and the discovery of multiple novel therapeutic approaches *(121-123)*. Despite all of these advances in the field, the role of constitutively active ACVR1 in the early inflammatory phase still remains unclear, prompting the development of additional injury models in alternative animal systems to address these open questions.

In our prior work, we developed the first adult zebrafish model for FOP *(91)*. We used Tol2 transgenesis to generate transgenic zebrafish carrying a heat-shock inducible, mCherry-tagged, constitutively active form of a*cvr1l*, the functional zebrafish ortholog of human *ACVR1*. We exposed these Acvr1l^{Q204D}-expressing animals to several months of daily heat shock to investigate whether the presence of constitutively active Acvr1l promoted the formation of FOP-like phenotypes. We found that adult zebrafish can ubiquitously express Acvr1l^{Q204D} when exposed to long-term daily heat-shock. Zebrafish expressing Acvr1l^{Q204D} develop FOP-like characteristics, including fully penetrant abnormal spinal curvature, and partially penetrant vertebral fusions, pelvic fin malformations, and HO lesions.

In this study, we expand upon our work with the *Tg(acvr1l_Q204D*) zebrafish, testing a series of injury models to investigate whether Acvr1l^{Q204D}-expressing zebrafish

can develop reliable site-directed HO lesions. We found that injury of Acvr1l^{Q204D}-expressing animals by any one of three methods, injection of recombinant human (rh) activin A, injection of cardiotoxin (CTX), or clipping of the caudal fin, resulted in early tissue damage that resolved normally and left no trace of HO at the site of injury. Despite this finding, several Acvr1l^{Q204D}-expressing animals, injured either by CTX injection or caudal fin clip, did develop HO lesions distal to the injury site, in the body cavity or along the spine. Here we describe the development and characterization of each of these injury models and our future plans to create a more robust zebrafish model for FOP to address some of the open questions that remain in the study of human FOP.

3.2 Materials and Methods

3.2.1 Zebrafish husbandry

Zebrafish (*Danio rerio)* were raised in the Tufts Yelick Lab Zebrafish Facility at 28.5°C in a controlled, automated recirculating environment, with 14/10 hour light/dark cycle, as previously described *(107)*. Zebrafish of both sexes were used in this study, at ages indicated in the manuscript. We used the following mutant and transgenic strains: *Tg(Bre:GFP) (108)* and *Tg(Bre:*GFP*); Tg(hsp70l:acvr1l_Q204D-mCherry) (91).* The following shorthand names are used in this manuscript: *Tg(hsp70l:acvr1l_Q204D-mCherry)* is referred to as *Tg(acvr1l_Q204D)*, protein product as Acvr1l^{Q204D}.

3.2.2 Ethics statement

All experimental procedures on zebrafish embryos and larvae were approved by the Tufts University Institutional Animal Care and Use Committee (IACUC) and Ethics Committee.

3.2.3 Heat-shock procedures

Adult *Tg(Bre:GFP)* and *Tg(Bre:*GFP*); Tg(acvr1l_Q204D)* zebrafish were heat-shocked once daily for 1 hour at 38°C, as previously described *(91)*. Animals were maintained on heat-shock systems through the duration of each injury experiment. At collection time points, animals were lethally anaesthetized using 250 mg/L tricaine methanesulfonate (Argent Aquaculture, Redmond, WA, USA) and fixed prior to Micro-CT analysis or further processing for histological and/or immunohistochemical analyses.

3.2.4 Injury methods

Zebrafish were injured using one of the following three methods: rh activin A injection, CTX injection, or caudal fin clip. For the activin A injury experiments, zebrafish were non-lethally anesthetized with 150 mg/L tricaine methanesulfonate. Scales were removed from the right side of each animal, above the spine, anterior to the dorsal fin, and posterior to the skull. Zebrafish were directly injected at the site of scale removal with rh activin A (R&D Systems, Minneapolis, MN, USA) in dimethyl sulfoxide (DMSO), at a concentration of 100 µg/ml based on manufacturer recommendation, using a 100 µm opening microcapillary needle. Control animals were injected with DMSO. 2 µl of injection fluid was dispensed per animal using a FemtoJet microinjection station (Eppendorf, Hamburg, Germany). After injection, animals were recovered in fresh system water and then returned to their respective heat-shock tanks for continued daily heat-shock. Adult *Tg(Bre:GFP)* and *Tg(Bre:*GFP*); Tg(acvr1l_Q204D)* zebrafish used for activin A injury experiments were heat-shocked for 8 months prior to activin A injections. Activin A injected zebrafish were collected for fixation at the following time

points: 1 hour post-injury (hpi), 2 days post-injury (dpi), and 4 weeks post-injury (wpi). Zebrafish collected at each time point were analyzed by histology and IHC.

The CTX injury experiments were carried out essentially as described above for the rh activin A injury experiments. Zebrafish were directly injected with cardiotoxin from *naja pallida* (217503; Millipore, Burlington, MA, USA) in phosphate-buffered saline (PBS) at a concentration of 300 μg/mL based on previous published experiments in zebrafish embryos *(124)*. Control animals were injected with PBS. Adult *Tg(Bre:GFP)* and *Tg(Bre:*GFP*); Tg(acvr1l_Q204D)* zebrafish used for CTX injury experiments were heat-shocked for 10 months prior to CTX injections. CTX injected zebrafish were collected for fixation at the following time points: 2 dpi, 4 wpi, and 8 wpi. Zebrafish collected at each time point were analyzed by Micro-CT (8 wpi only), histology, and IHC.

For the caudal fin clip injury experiments, anesthetized zebrafish had ~50% of the caudal fin removed by cutting with a sterile razor blade. Bright field images of zebrafish pre- and post-fin clip were captured using an Axiocam 503 color camera (Zeiss, Oberkochen, Germany) attached to an M2-Bio dissecting microscope (Zeiss, Oberkochen, Germany) and processed using AxioVision SE64 microscopy software (Zeiss, Oberkochen, Germany). Adult *Tg(Bre:GFP)* and *Tg(Bre:*GFP*); Tg(acvr1l_Q204D)* zebrafish used for caudal fin clip injury experiments were heat-shocked for 7 months prior to fin clip injuries. Caudal fin clip-injured zebrafish were all collected for fixation at 2 wpi and analyzed by Micro-CT, histology, and IHC.

3.2.5 Histology and immunohistochemistry

Two different methods of fixation, tissue processing, and paraffin embedding were used on samples from the injury experiments. For the activin A and CTX injury experiments, animals were processed as previously described *(91)*. For tail clip injury experiments, animals were processed using an alternative protocol as previously described with modifications *(125)*. In brief, lethally anaesthetized adult zebrafish were fixed in 10% formalin in PBS for 48 hours at room temperature, then rinsed and stored in PBS at 4°C. To process for paraffin embedding, samples were decalcified in CalEx (Fisher Scientific, Pittsburgh, PA, USA) and then rinsed in PBS for 2 hours. Samples were immersed for 1 hour in 50% ethanol, overnight in 75% ethanol, then in a graded t-butyl alcohol series for 1 hour each. Samples were transferred to molten Paraplast Plus paraffin (McCormick Scientific, St. Louis, MO, USA) and allowed to equilibrate overnight. Samples were embedded in fresh molten paraffin and allowed to solidify at room temperature. Paraffin blocks were serially sectioned at 7 μm and mounted on SuperFrost Plus charged glass microscope slides (Fisher Scientific, Pittsburgh, PA, USA).

For histological analyses, mounted sections were stained with H&E or Safranin O with a Fast Green counter stain. For Safranin O staining, slides were submerged in 0.02% Fast Green in 0.2% acetic acid for 15 seconds followed directly by submersion in 1% Safranin O for 30 seconds. Paraffin sections used for IHC analyses were processed as previously described *(91)*. Sections were counterstained with 0.02% Fast Green in 0.2% acetic acid for 15 seconds. For IHC analyses, the following antibodies were used: 1:200 goat anti-activin A (AF338; R&D Systems, Minneapolis, MN, USA); 1:100 goat anti-

Collagen I (AB758; Millipore, Burlington, MA, USA); 1:200 rabbit anti-Collagen II (ab34712; Abcam, Cambridge, MA, USA); 1:250 rabbit anti-pSmad2 (AB3849-I; Millipore, Burlington, MA, USA); 1:50 rabbit anti-vWF (HPA001815; Sigma-Aldrich, St. Louis, MO, USA); 1:500 donkey anti-rabbit and 1:500 donkey anti-goat (Jackson ImmunoResearch Laboratories, West Grove, PA, USA). All stained slides were visualized using a Zeiss AxioPhot epifluorescence microscope (Zeiss, Oberkochen, Germany). Images were captured using an Axiocam 503 color camera (Zeiss, Oberkochen, Germany) and processed using AxioVision SE64 microscopy software (Zeiss, Oberkochen, Germany).

3.2.6 Micro-computed tomography (Micro-CT)

Euthanized adult zebrafish were imaged using a Skyscan 1176 high-resolution micro-CT Scanner (Bruker, Allentown, PA, USA) as previously described *(91)*. Scans were completed at 9 μm resolution, every 0.5 degrees over 180 degrees. Reconstructions were completed using NRecon (Bruker, Allentown, PA, USA) and 3D volume renderings were generating using CTVox (Bruker, Allentown, PA, USA). All reconstruction and rendering settings were kept constant between samples to allow for comparison.

3.2.7 Methodology and Statistics

All animals established on a given heat-shock system that were part of injury experiments were included in analyses described below. Animal numbers are indicated in figure legends. Only animals that died of natural causes prior to desired collection time point were excluded from analyses.

3.3 Results

3.3.1 Delivery of rh activin A does not induce HO formation in heat-shocked Tg(acvr1l_Q204D) zebrafish at injury site

In order to induce HO formation in a reliable, reproducible site-directed manner, many researchers have turned to various methods of injury in mouse models of FOP *(18, 34, 38, 46, 47, 55, 86, 120-123)*. We chose to apply similar methods to our Acvr1l^{Q204D}-expressing zebrafish with the goal of identifying one or more effective means for inducing HO formation. We began our injury experiments with the injection of rh activin A, as it was recently identified as a critical ligand for ACVR1^{R206H}-driven HO formation in an FOP mouse model *(18)*. As there are few existing protocols for the delivery of compounds in liquid to adult zebrafish muscle tissue, we developed our own method. In brief, adult zebrafish were anesthetized and scales were removed from the upper right side, posterior to the skull and anterior to the dorsal fin (Figure 3.1A) to provide an exposed area of skin. 2 μL of either 100 μg/mL rh activin A or DMSO vehicle control was injected into the muscle tissue using a microcapillary needle (Figure 3.1B) and then animals were recovered in fresh system water. For our first round of injections, we tested whether we could detect the presence of rh activin A in the muscle tissue of *Tg(Bre:GFP)* animals at 1 hpi using paraffin section IHC (Figure 3.1C–H). rh activin A was detected in the muscle tissue of rh activin A-injected animals (Figure 3.1E, H), but not in DMSO-injected animals (Figure 3.1D, G). rh activin A was also absent in samples lacking the primary antibody (Figure 3.1C, F).

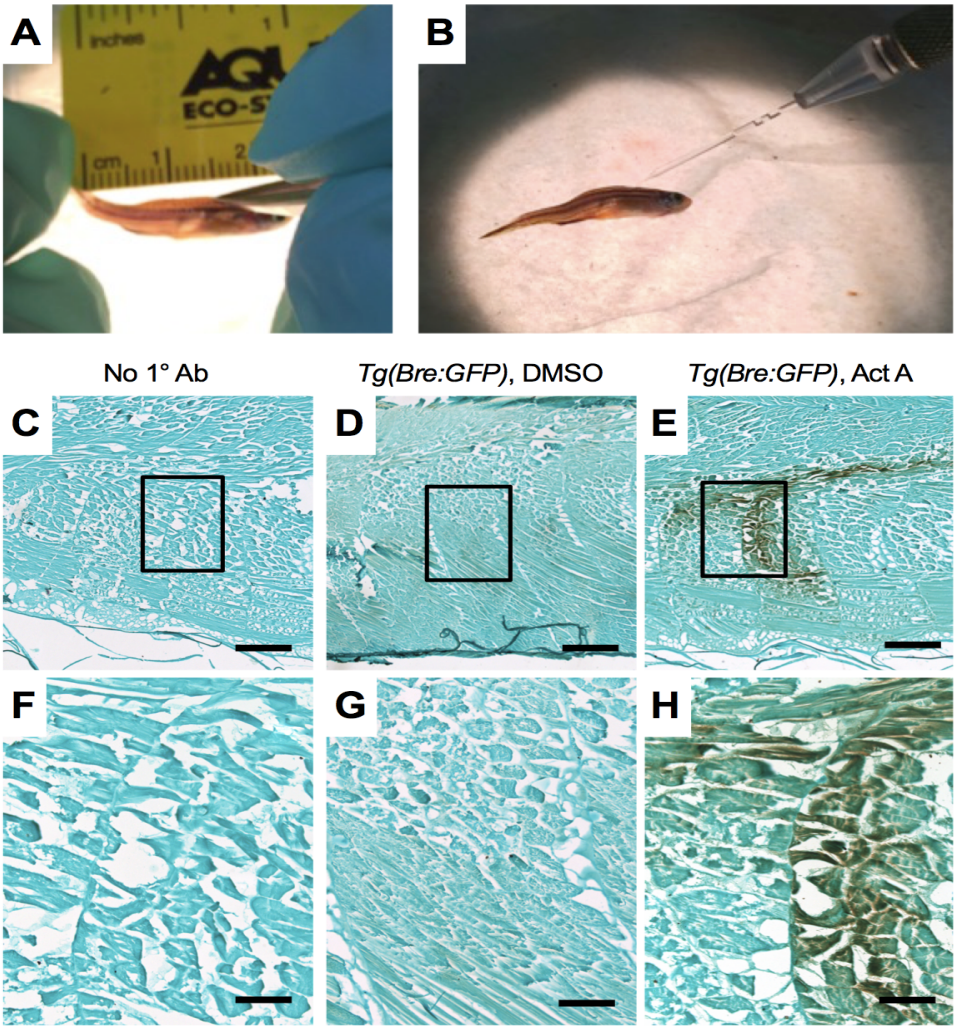

Figure 3.1. rh activin A is detectable in zebrafish muscle tissue at 1 hpi. For injection injury experiments, adult zebrafish were anesthetized, their scales were removed from the upper right side, anterior to the dorsal fin (A), and they were injected with the indicated treatment using a microcapillary needle (B). Adult *Tg(Bre:GFP)* zebrafish injected with rh activin A (E: 5x, H: 20x) or DMSO (D: 5x, G: 20x) were collected at 1 hpi, paraffin sectioned, and analyzed for rh activin A expression by IHC. No primary controls were negative (C: 5x, F: 20x). (F–H) are enlarged views of areas indicated by boxes in (C–E), respectively. n = 2 zebrafish per treatment group. (C–E) 5x scale bar is 200 μm. (F–H) 20x scale bar is 50 μm. Act A, activin A, hpi, hours post-injury, IHC, immunohistochemistry.

After confirming the effective delivery of rh activin A to zebrafish muscle tissue, we proceeded to perform rh activin A injections on adult heat-shocked *Tg(Bre:GFP)* and *Tg(Bre:*GFP*); Tg(acvr1l_Q204D)* zebrafish. Animals were collected at 2 dpi and 4 wpi and each injection site was analyzed using H&E staining and IHC (Figure 3.2). The collection at 2 dpi was intended to confirm the presence of muscle tissue damage at the site of injury, while the collection at 4 wpi was intended for detection of HO formation, based on the knowledge that HO typically develops within 3 weeks of injury in FOP mouse models *(18, 51, 85)*. At 2 dpi, all of the animals displayed clear tissue damage at the site of injury in response to either rh activin A or DMSO injection (Figure 3.2A–D, damage denoted by dashed lines). Staining for nuclear pSmad2 indicated similar levels of activation of TGFβ signaling in all animals (Figure 3.2E–H). TGFβ signal activation is a normal response to injury in many systems *(126, 127)*, including zebrafish *(128)*. By 4 wpi, heat-shocked *Tg(Bre:GFP)* and *Tg(Bre:*GFP*); Tg(acvr1l_Q204D)* zebrafish showed normal healing and resolution of the tissue damage (Figure 3.2I–L), regardless of the injected compound. These results indicate that injection of rh activin A does not promote the formation of HO in Acvr1l^{Q204D}-expressing zebrafish.

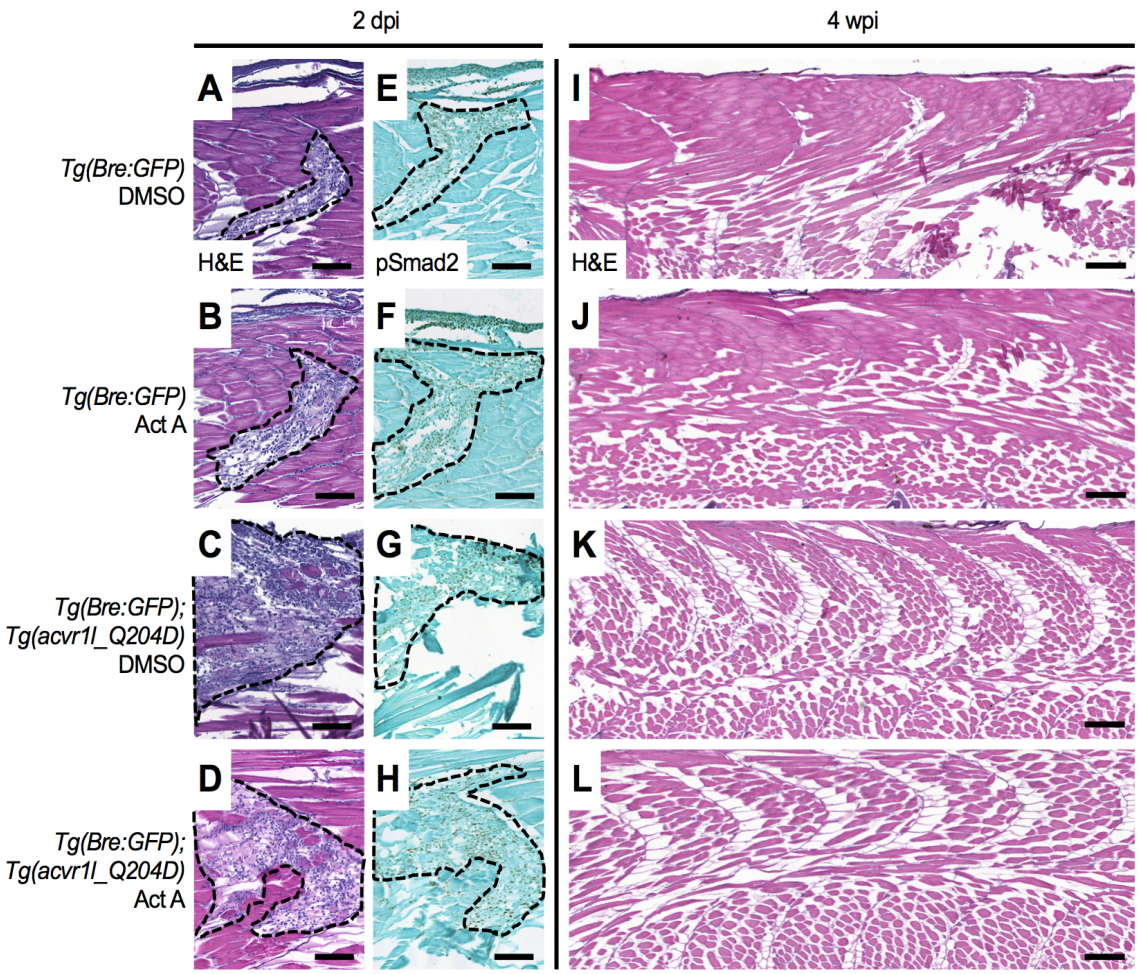

Figure 3.2. rh activin A injection causes tissue damage at 2 dpi that resolves by 4 wpi. Adult heat-shocked *Tg(Bre:GFP)* and *Tg(Bre:GFP); Tg(acvr1l_Q204D-mCherry)* zebrafish injected with rh Activin A (B, D, F, H, J, L) or DMSO (A, C, E, G, I, K) were collected at 2 dpi (A–H) and 4 wpi (I–L). Paraffin sections were analyzed by H&E staining (A–D, I-L) and anti-pSmad2 IHC (E–H). Extent of tissue damage marked by dashed line in (A–H). n = 2 zebrafish per treatment group, per time point. (A–H) 20x scale bar is 100 µm. (I–L) 5x scale bar is 200 µm. Act A, activin A, dpi, days post-injury, IHC, immunohistochemistry, wpi, weeks post-injury.

3.3.2 Delivery of CTX does not induce HO formation in heat-shocked Tg(acvr1l_Q204D) zebrafish at injury site

We next tested whether injection of CTX would induce HO formation in Acvr1l^{Q204D}-expressing zebrafish. Cardiotoxin injection has been used previously in zebrafish embryos to study muscle regeneration *(124)* and numerous times in mouse models of FOP *(38, 46, 47, 55, 86, 120, 121, 123)*. This toxin causes strong muscle fiber contraction and degradation *(129)*. CTX injections were conducted in a similar manner to rh activin A injections: heat-shocked *Tg(Bre:GFP)* and *Tg(Bre:*GFP*); Tg(acvr1l_Q204D)* zebrafish were anesthetized, descaled, injected with 1 μL of either 300 μg/mL CTX or PBS vehicle control using a microcapillary needle, and then recovered in system water. Animals were collected at 2 dpi and 4 wpi and each injection site was analyzed using histology and IHC (Figure 3.3A–L). At 2 dpi, all of the animals displayed tissue damage at the site of injury (Figure 3.3A–D, damage denoted by dashed lines) that was similar in appearance to that seen with rh activin A injection (Figure 3.2). Notably, the tissue damage caused by CTX injection (Figure 3.3B, D) into both *Tg(Bre:GFP)* and *Tg(Bre:*GFP*); Tg(acvr1l_Q204D)* zebrafish was larger in size than the damage generated by PBS control injection (Figure 3.3A, C). pSmad2 staining was used to confirm activation of TGFβ signaling throughout the damaged tissue of each animal, with no significant differences in pSmad2 levels detected between treatment groups (Figure 3.3E–H). By 4 wpi, the tissue damage caused by CTX injection had resolved completely and the muscle returned to its normal appearance in *Tg(Bre:GFP)* and *Tg(Bre:*GFP*); Tg(acvr1l_Q204D)* zebrafish (Figure 3.3I, J). The dark red Safranin O staining indicative of cartilaginous proteoglycans, a hallmark of HO lesions, was noticeably absent at the

site of injury in zebrafish of either genotype (Figure 3.3K, L). These results suggest that Acvr1l^{Q204D}-expressing zebrafish do not form HO at the site of CTX injury.

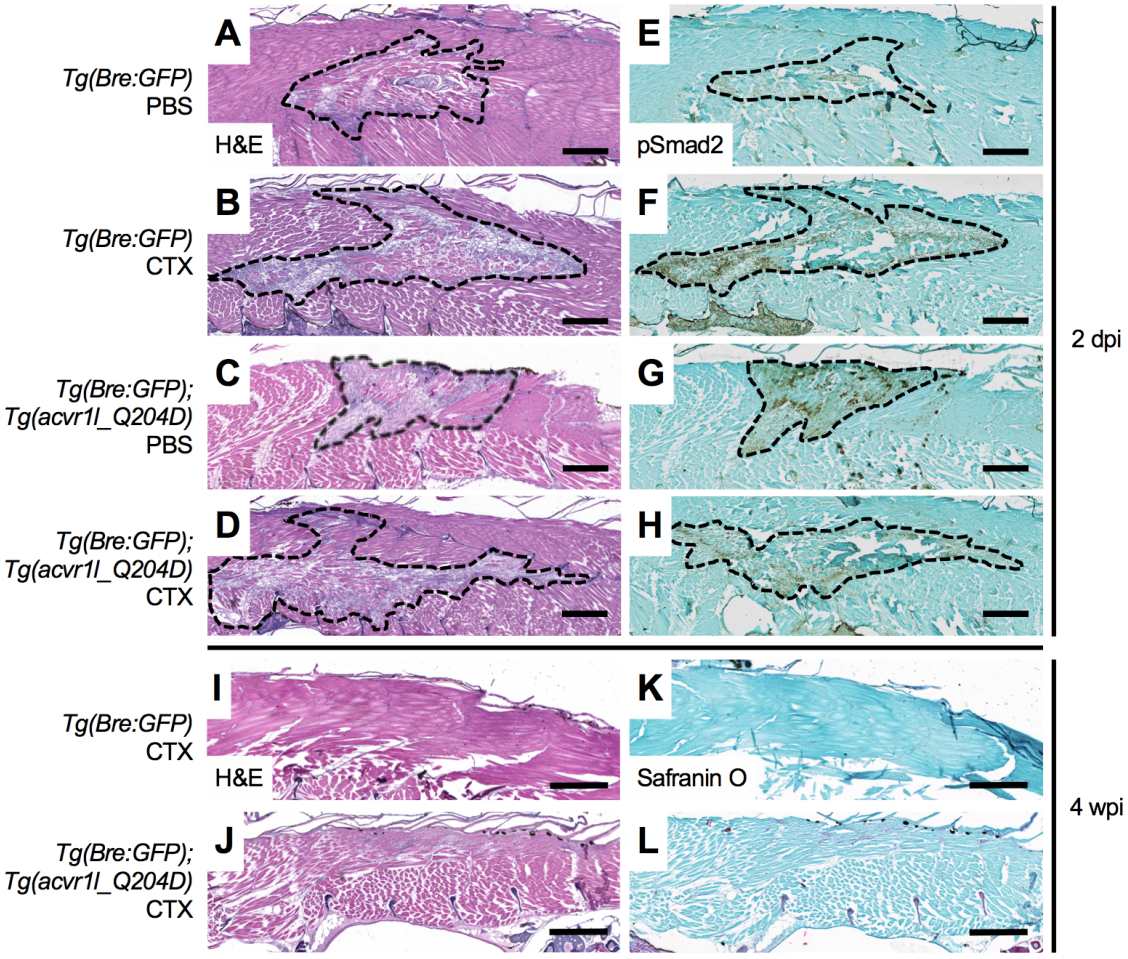

Figure 3.3. Cardiotoxin injection causes tissue damage at 2 dpi that resolves by 4 wpi. Adult heat-shocked *Tg(Bre:GFP)* and *Tg(Bre:GFP); Tg(acvr1l_Q204D-mCherry)* zebrafish injected with cardiotoxin (B, D, F, H, I–L) or PBS (A, C, E, G) were collected at 2 dpi (A–H) and 4 wpi (I–L). Paraffin sections were analyzed by H&E staining (A–D, I, J), Safranin O staining (K, L), and anti-pSmad2 IHC (E–H). Extent of tissue damage marked by dashed line in (A–H). n = 1 zebrafish per PBS treatment group, 3 zebrafish per CTX treatment group at 2 dpi. n = 1 zebrafish per CTX treatment group at 4 wpi. (A–L) 5x scale bar is 400 μm. CTX, cardiotoxin, dpi, days post-injury, IHC, immunohistochemistry, wpi, weeks post-injury.

3.3.3 HO formation is observed in body cavity of CTX-injured heat-shocked Tg(acvr1l_Q204D) zebrafish

A cohort of CTX-injured *Tg(Bre:GFP)* and *Tg(Bre:*GFP*); Tg(acvr1l_Q204D)* zebrafish were collected at 8 wpi and analyzed by Micro-CT to determine whether the Acvr1l^{Q204D}-expressing animals harbored any detectable HO (Figure 3.4A–D). Of the three Acvr1l^{Q204D}-expressing zebrafish analyzed at 8 wpi, one displayed densely mineralized HO lesions within the body cavity (arrows in Figure 3.4C, D) that was reminiscent of HO lesions observed during the initial characterization of the *Tg(Bre:*GFP*); Tg(acvr1l_Q204D)* zebrafish *(91)*. The *Tg(Bre:GFP)* zebrafish did not develop any HO (Figure 3.4A, B). The Acvr1l^{Q204D}-expressing animal was paraffin embedded and sectioned so that the HO lesions could be further evaluated by histological staining (Figure 3.4E–H). H&E staining revealed a highly heterogenous HO lesion (Figure 3.4E, F), while Safranin O staining confirmed the presence of regions of cartilage matrix deposition within the lesion (Figure 3.4G, H).

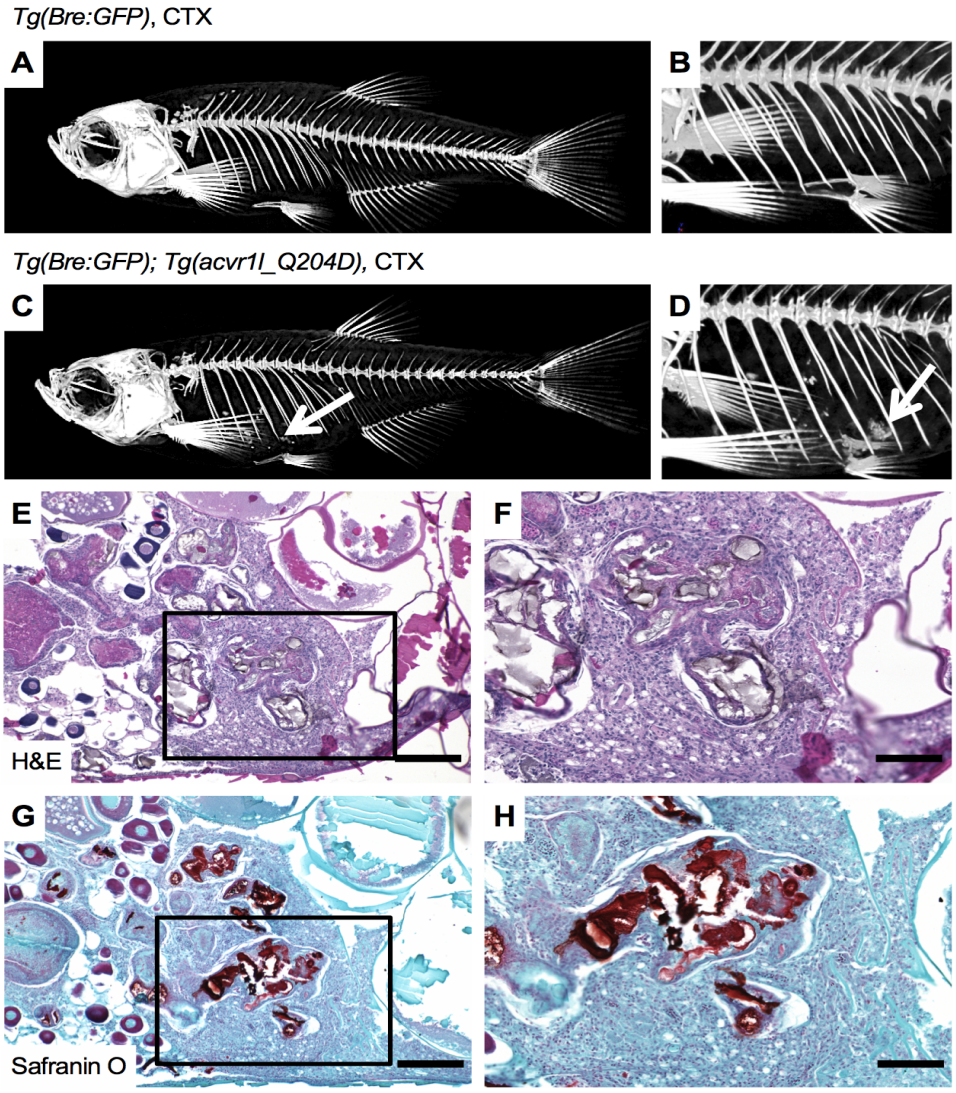

Figure 3.4. Cardiotoxin-injected heat-shocked *Tg(acvr1l_Q204D)* zebrafish develop body cavity HO by 8 wpi. Micro-CT imaging of cardiotoxin-injected heat-shocked *Tg(Bre:GFP); Tg(acvr1l_Q204D-mCherry)* zebrafish (C, D) at 8 wpi revealed the presence of HO in the body cavity (arrows in C, D). Control cardiotoxin-injected heat-shocked *Tg(Bre:GFP)* zebrafish did not exhibit this phenotype (A, B). H&E (E, F) and Safranin O (G, H) staining revealed the heterogeneity of the HO, including numerous proteoglycan-dense regions (G, H, strong red Safranin O stain). (F, H) are enlarged views of areas indicated by boxes in (E, G), respectively. n = 3 *Tg(Bre:GFP); Tg(acvr1l_Q204D-mCherry)* zebrafish with CTX treatment. n = 1 *Tg(Bre:GFP)* zebrafish with CTX treatment. (E, G) 10x scale bar is 200 µm. (F, H) 20x scale bar is 100 µm. CTX, cardiotoxin, HO, heterotopic ossification, wpi, weeks

3.3.4 Caudal fin clip does not induce HO formation in heat-shocked Tg(acvr1l_Q204D) zebrafish at injury site

For our third injury model, we moved away from injection experiments and turned to a well-established method of injury in the zebrafish, caudal fin clip *(107)*. In brief, *Tg(Bre:GFP)* and *Tg(Bre:*GFP*); Tg(acvr1l_Q204D)* zebrafish were anesthetized and imaged by bright field microscopy prior to caudal fin clip (Figure 3.5A, B) and then a sterile razorblade was used to remove ~50% of the caudal fin tissue (Figure 3.5C, D). Animals were recovered in system water and monitored for proper fin regeneration at 1 wpi (Figure 3.5E, F) and 2 wpi (Figure 3.5G, H). Animals were collected and analyzed by Micro-CT at 2 wpi (Figure 3.5I, J). Gross inspection by bright field imaging and analysis of mineralization by Micro-CT revealed that all *Tg(Bre:GFP)* and *Tg(Bre:*GFP*); Tg(acvr1l_Q204D)* zebrafish showed normal caudal fin regeneration and no signs HO formation at the site of injury by 2 wpi.

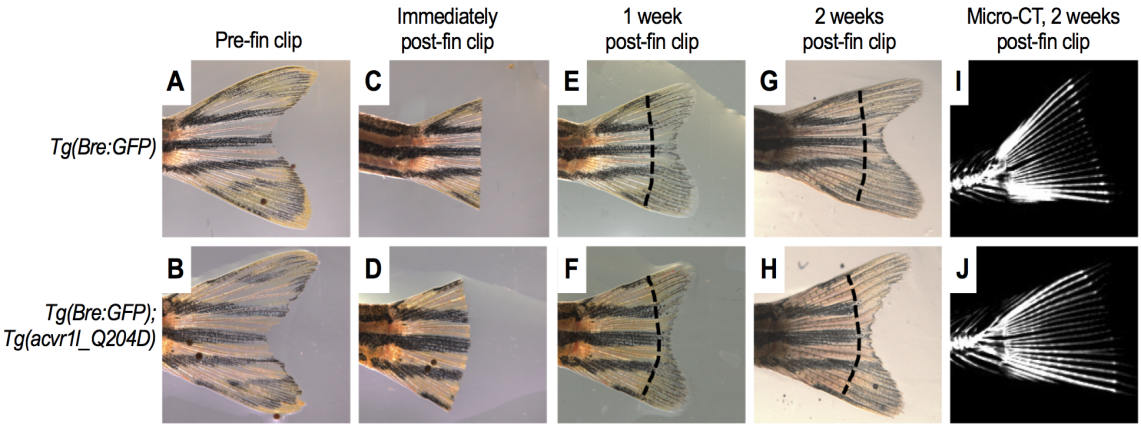

Figure 3.5. Caudal fin clip does not result in HO formation at injury site in heat-shocked *Tg(acvr1l_Q204D)* zebrafish by 2 wpi. For caudal fin clip injury experiments, adult heat-shocked *Tg(Bre:GFP)* and *Tg(Bre:GFP); Tg(acvr1l_Q204D-mCherry)* zebrafish were imaged with bright field microscopy just prior to fin clip (A, B), immediately after fin clip (C, D), at 1 wpi (E, F), and at 2 wpi (G, H). Original site of fin clip marked by dashed line in (E–H). Zebrafish were also imaged by Micro-CT (I, J) at 2 wpi. n = 3 zebrafish per genotype. HO, heterotopic ossification, wpi, weeks post-injury.

3.3.5 HO formation is observed along spine and in body cavity of fin clip-injured heat-shocked Tg(acvr1l_Q204D) zebrafish

Further inspection of the whole animal Micro-CT renderings of the caudal fin clip-injured *Tg(Bre:GFP)* and *Tg(Bre:*GFP*); Tg(acvr1l_Q204D)* zebrafish uncovered the development of numerous HO lesions in two of the three Acvr1l^{Q204D}-expressing zebrafish (Figure 3.6D–I). One of the Acvr1l^{Q204D}-expressing animals developed small HO lesions within the body cavity and rod-like HO directly adjacent to the spine (arrows in Figure 3.6D–F), while the other developed a single large HO lesion within the body cavity (arrows in Figure 3.6G–I). None of the *Tg(Bre:GFP)* zebrafish showed any signs of HO formation (Figure 3.6A–C).

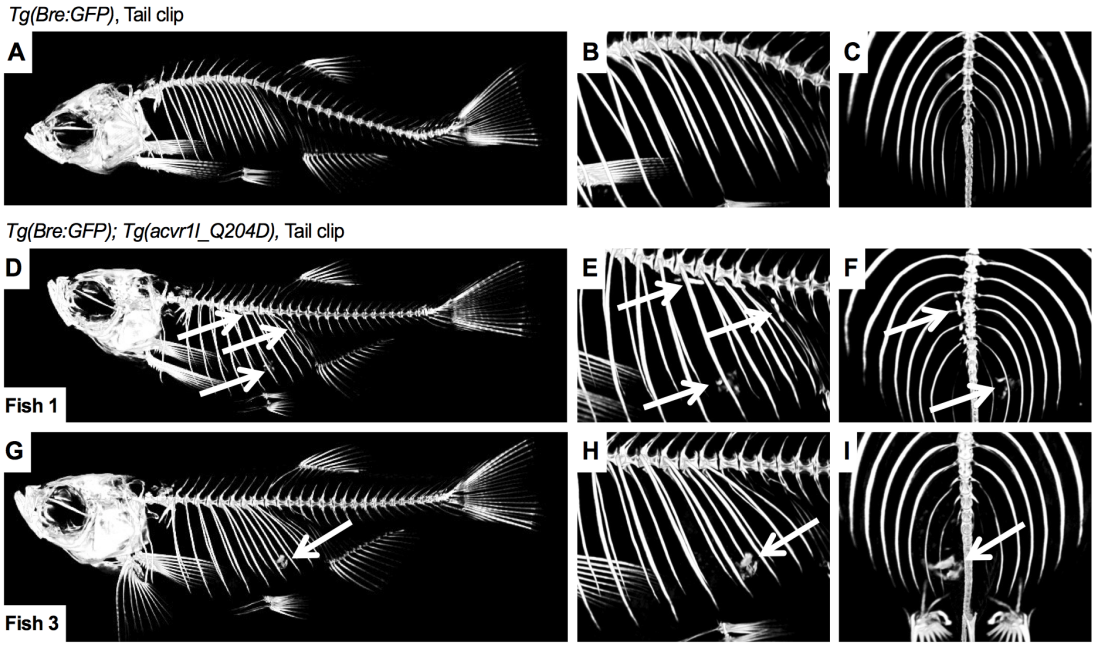

Figure 3.6. Caudal fin clip-injured heat-shocked *Tg(acvr1l_Q204D)* zebrafish develop spinal and body cavity HO by 2 wpi. Micro-CT imaging of fin clip-injured heat-shocked *Tg(Bre:GFP); Tg(acvr1l_Q204D-mCherry)* zebrafish (D–I) at 2 wpi revealed the presence of HO in the body cavity and along the spine (arrows in D–I). Control fin clip-injured heat-shocked *Tg(Bre:GFP)* zebrafish did not exhibit this phenotype (A–C). n = 3 *Tg(Bre:GFP); Tg(acvr1l_Q204D-mCherry)* zebrafish. n = 1 *Tg(Bre:GFP)* zebrafish. HO, heterotopic ossification, wpi, weeks post-injury.

The Acvr1l^{Q204D}-expressing zebrafish that displayed HO lesions were further processed by paraffin embedding and sectioning and analyzed by H&E staining (Figure 3.7A, B, F, G) and IHC (Figure 3.7C–E, H–J). H&E staining showed the extent of each HO lesion in the Acvr1l^{Q204D}-expressing animals (Figure 3.7A, F, lesion denoted by dashed lines), while higher magnification imaging revealed the heterogeneity of each lesion (Figure 3.7B, G). IHC was used on adjacent sections to confirm the presence of several cell types commonly found in HO. Positive staining for vWF (Figure 3.7C, H) indicated the infiltration of endothelial cells, while positive Collagen II (Figure 3.7D, I) and Collagen I (Figure 3.7E, J) staining revealed the deposition of cartilage and bone matrix, respectively. Interestingly, each marker shows positive staining within different regions of the HO lesions, suggesting that different regions are a reflection of various stages that occur during the process of HO development.

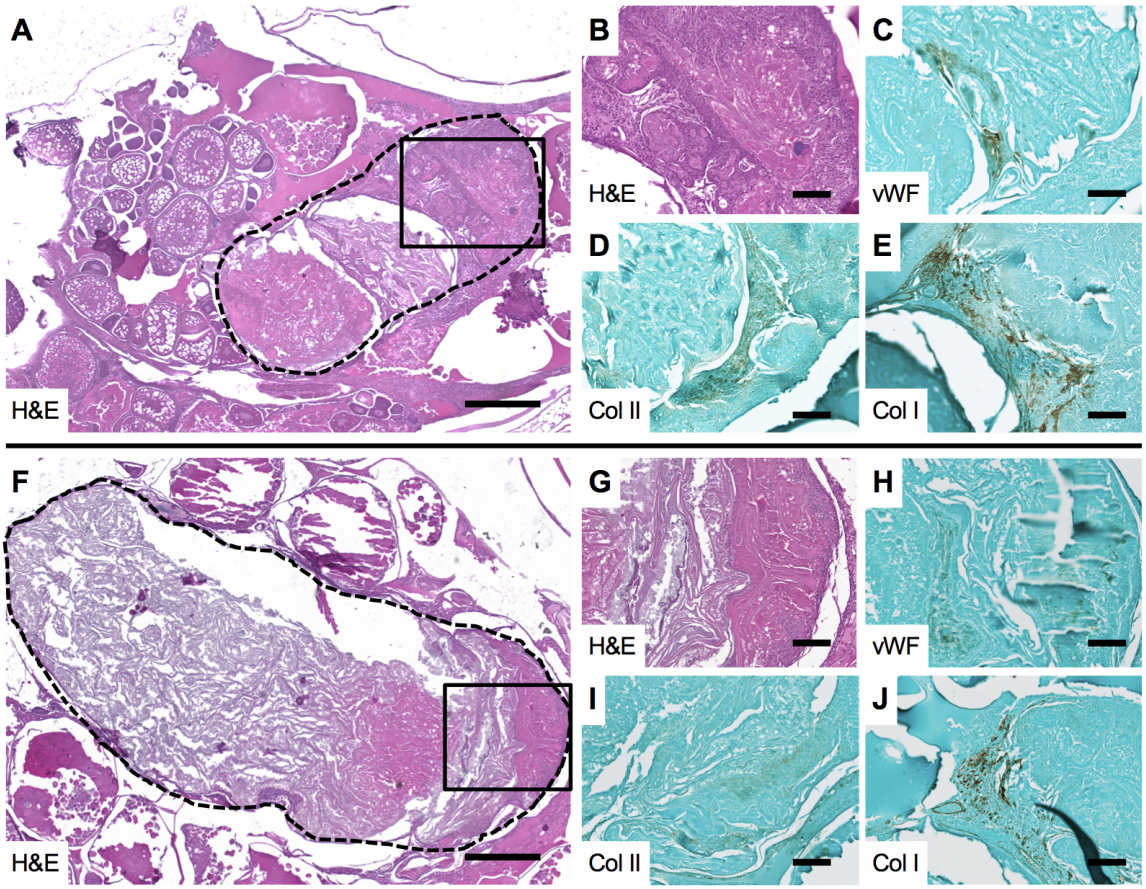

Figure 3.7. Body cavity HO expresses markers of cartilage and bone. HO lesions from fin clip-injured heat-shocked *Tg(Bre:GFP); Tg(acvr1l_Q204D-mCherry)* zebrafish at 2 wpi were paraffin sectioned and analyzed by H&E staining (A, B, F, G) and IHC for vWF (C, H), Col II (D, I), and Col I (E, J). Outline of HO lesion marked by dashed line in (A, F). (B, G) are enlarged views of areas indicated by boxes in (A, F), respectively. (A, F) 5x scale bar is 400 μm. (B–E, G–J) 20x scale bar is 100 μm. Col I, Collagen I, Col II, Collagen II, HO, heterotopic ossification, IHC, immunohistochemistry, vWF, von Willebrand factor, wpi, weeks post-injury.

3.4 Discussion

In this study, we describe the development and characterization of several injury methods using previously validated *Tg(acvr1l_Q204D)* zebrafish as a model for human FOP *(91)*. Injury of adult zebrafish expressing the heat-shock-inducible Acvr1l^{Q204D} with rh activin A, CTX, or caudal fin clip results in early signs of tissue damage but does not manifest in HO lesion formation at the site of injury. Instead, these animals developed HO at sites distal to each injury, within the body cavity or along the spine. These lesions resemble those seen in the initial characterization of the *Tg(acvr1l_Q204D)* zebrafish *(91)*, though they are larger in size. These results suggest that while *Tg(acvr1l_Q204D)* zebrafish do continue to acquire key hallmarks of FOP, they do not respond to injury by developing reliable site-directed HO, and that a more robust zebrafish model will need to be established to permit the study of early events in HO lesion formation in FOP.

We first saw that *Tg(acvr1l_Q204D)* zebrafish injected with rh activin A did not respond by forming HO at the site of injury. There are several potential explanations for this finding. It is possible that rh activin A does not bind to the zebrafish Acvr1l receptor as it does mouse ACVR1 and human ACVR1. The amino acid sequence of full-length zebrafish Acvr1l is 69% identical to human ACVR1 and, in particular, the intracellular serine/threonine kinase domain is 85% identical, strongly suggesting the conservation of receptor function in intracellular signaling cascades *(21, 65)*. However, the extracellular ligand binding domain is only 30.3% conserved *(65)*, implying a divergence of function for this region through evolutionary time. In addition, the zebrafish inhibin β_A subunits that dimerize to form activin A are only 55% identical to the human inhibin β_A subunits. Indeed, the lack of staining for zebrafish activin A by the anti-rh activin A antibody seen

in the DMSO injected control zebrafish (Figure 3.1D, G) indicates a lack of conservation of this protein sequence that prohibits antibody binding. These findings suggest that zebrafish Acvr1l may not be capable of binding and responding to the presence of rh activin A with the formation of HO lesions.

Another possible explanation lies in our use of zebrafish expressing Acvr1l^{Q204D}. Previous work has shown that the p.Q204D/Q207D mutation is ligand independent *(13)*. Indeed, recent work has suggested that the p.Q207D mutation is unaffected by activin A binding, such that the ligand can neither suppress nor stimulate further activity of the ACVR1 receptor *(130)*. Therefore, it is also possible that our use of *Tg(acvr1l_Q204D)* zebrafish obstructed our ability to observe the formation of HO in response to injection of rh activin A.

We next observed that neither injection of CTX nor caudal fin clip injury in *Tg(acvr1l_Q204D)* zebrafish was capable of initiating HO formation at the site of injury. Despite observing clear tissue damage at early time points in each model, this damage never evolved into full-blown HO at later time points. We hypothesize that this could be due to the unique regenerative abilities of zebrafish, which belong to a small group of vertebrate organisms capable of regeneration of adult tissues. Zebrafish have a well-studied capacity to regenerate a number of tissues as adults, including the fins, heart, retina, and spinal cord (reviewed in *(131)*. In contrast, adult mammals have very limited regenerative capacity. It is possible that some of the signaling programs activated during tissue regeneration in the zebrafish can dampen or completely block the effects of constitutive activation of Acvr1l. For example, retinoic acid (RA) and the RA signaling pathway are upregulated in early stages of zebrafish fin regeneration and play a key role

in the establishment of the blastema *(132)*. In models of HO development, RA has been shown to act upon RA receptor gamma (RARγ) to inhibit BMP signaling through Smad1/5/8 so that infiltrating fibroproliferative cells do not undergo chondrogenesis and osteogenesis *(54, 55, 133)*. In fact, the RARγ agonist palovarotene is capable of preventing HO formation in FOP mouse models *(55, 56)* and has shown some potential as a therapeutic in clinical trials with human FOP patients (http://www.prnewswire.com/news-releases/phase-2-part-a-open-label-extension-trial-of-palovarotene-for-treatment-of-patients-with-fibrodysplasia-ossificans-progressiva-continues-positive-trends-300429975.html). Future studies may investigate whether $Acvr1l^{Q204D}$-expressing zebrafish are capable avoiding injury-induced HO formation by activating RA signaling in response to injury.

In both the CTX injury model and the caudal fin clip injury model, however, HO was observed in regions distal to the site of injury. It is possible, and perhaps likely, that the HO seen in these animals was present prior to injury. It is also possible that each of these injuries contributed to some level of heightened systemic inflammation that significantly increased the size of each lesion, when compared to HO characterized in uninjured *Tg(acvr1l_Q204D)* zebrafish *(91)*. This finding would support recent work describing the presence of amplified inflammation directly preceding mineralization and the finding that existing HO begets more HO *(85)*. While information about systemic inflammation status was not gathered in these experiments, future injury experiments could incorporate the use of MRI to visualize inflammation and edema and correlate surges in these processes with enhanced HO formation, confirming some level of efficacy of injury models in the development of HO lesions in the *Tg(acvr1l_Q204D)* zebrafish.

While the p.Q204D/Q207D mutation used to establish our zebrafish FOP model *(91)*, as well as other mouse FOP models *(33, 35, 55, 82, 84)*, does cause the development of FOP-like phenotypes in these models, it is not a naturally occurring mutation in human FOP patients. In addition, this mutation promotes constitutive activation of ACVR1 in a ligand-independent fashion, unlike the p.R206H and p.Q207E mutations, and has been shown to cause significantly more severe phenotypes than the FOP-associated mutations *(13)*. Therefore, future work will focus on the generation of zebrafish carrying the p.R206H mutation found in ~90% of human FOP patients *(8, 134)*. A dual-pronged approach will be used to generate these animals. For the first method, the p.R203H mutation will be introduced into the existing Tol2 *hsp70l:acvr1l-mCherry* vector using site-directed mutagenesis and then transgenic animals expressing heat-shock inducible *Tg(hsp70l:acvr1l_R203H-mCherry)* will be created using Tol2 transgenesis, as previously described *(91)*. For the second method, the endogenous zebrafish *Acvr1l* locus will be targeted using CRISPR and the p.R203H mutation will be introduced by homology directed repair. It is anticipated that at least one, if not both, of these approaches will provide a zebrafish model for FOP that more accurately reflects the human disease and may develop HO in response to injury.

In summary, this study reveals that heat-shocked *Tg(acvr1l_Q204D)* zebrafish display an intriguing difference in response to injury when compared to mouse models of FOP. These results could suggest additional functional differences between the artificial p.Q204D mutation and patient-associated mutations or they could reflect a fundamental difference in the biology of wound healing between zebrafish and mammals. Future

studies will address this question and determine whether a novel mechanism of healing in the zebrafish could be exploited for the benefit of human FOP patients.

Chapter 4: Discussion

In this thesis, I describe our work to date generating, characterizing, and manipulating the first adult zebrafish model for FOP. FOP is a rare genetic disease that manifests in skeletal malformation and progressive HO formation and is caused by activating mutations in the gene *ACVR1*. Zebrafish possess a functional ortholog of human *ACVR1*, called *Acvr1l*. We created zebrafish that express heat-shock-inducible, constitutively active Acvr1l (Acvr1l^{Q204D}) to assess the development of FOP-like phenotypes in adult animals. We observed that heat-shocked Acvr1l^{Q204D}-expressing adult zebrafish develop a variety of fully and partially penetrant FOP-like phenotypes, including HO, fused vertebrae, pelvic fin malformations, and abnormal spinal lordosis *(91)*. We proceeded to use the Acvr1l^{Q204D}-expressing animals to develop several injury models for the purpose of inducing reliable site-directed HO formation. Using rh activin A, cardiotoxin, and caudal fin clip, we consistently observed that injury of heat-shocked Acvr1l^{Q204D}-expressing animals did not result in HO formation at the site of injury. However, we did note that several of these animals exhibited HO at other sites throughout the body. From the sometimes unexpected, but certainly interesting, results of our experiments, we have concluded that heat-shock-inducible *Tg(acvr1l_Q204D)* zebrafish can serve as a useful tool for studying human FOP and may provide an opportunity to identify fundamental differences in wound healing between zebrafish and mammals.

One of our key goals for the future is to generate zebrafish that harbor the p.R203H/R206H mutation found in ~90% of human FOP patients *(8, 134)*. Several studies have recently shown that the altered ligand response of ACVR1 to activin A that

is key for the progression of FOP lesion formation is specific to naturally occurring FOP mutations, such as the p.R206H and p.Q207E mutations *(13, 85, 134)*. The p.Q204D/Q207D promotes constitutive activation of ACVR1 in a ligand-independent manner *(13)*. So while animal models that harbor the p.Q204D/Q207D mutation do develop FOP-like phenotypes *(33, 35, 55, 82, 84, 91)*, they may not be providing the most robust representation of human FOP.

To this end, we have begun to use two different approaches to introduce the p.R203H mutation into zebrafish. Our first approach involves modifying our existing Tol2 *hsp70l:acvr1l-mCherry* vector using site-directed mutagenesis to insert the p.R203H mutation. This vector will be injected into single-cell zebrafish embryos with the Tol2 transposase to promote genomic integration and generate transgenic animals harboring heat-shock inducible *Tg(hsp70l:acvr1l_R203H-mCherry)*. These adult animals will be exposed to long-term heat-shock much like the *Tg(hsp70l:acvr1l_Q204D-mCherry)* zebrafish in order to assess the development of FOP-like phenotypes. Our second approach takes advantage of the relative ease of performing CRISPR/Cas9-based gene editing in zebrafish. We will identify guide RNAs that promote Cas9-mediated cutting of the endogenous zebrafish *Acvr1l* locus near the site of the p.R203H mutation. Once effective guide RNAs are in hand, we will attempt to use homology directed repair to introduce the p.R203H mutation at the endogenous locus. We expect that zebrafish harboring Acvr1l^{R203H} will serve as a more accurate model of human FOP.

Another goal for the future is to perform genetic modifier screens in our zebrafish FOP model that allow for the identification of gene mutations that either suppress or intensify FOP disease progression. Human patients with FOP show significant variability

in the onset of FOP-associated symptoms, in the rate of their progression, and in the severity their symptoms *(4)*. Our clinician collaborators from the Hsiao lab at the University of California in San Francisco have done extensive natural histories of dozens of FOP patients and found that a subset of patients show significantly suppressed disease progression. Together, we speculate that these patients possess uncharacterized genetic mutations that somehow subdue the overactivation of BMP signaling caused by constitutive activation of ACVR1 and lead to milder symptoms. By performing sequencing on these patient samples, we can identify candidate gene mutations that could be responsible for disease suppression. These gene mutations are best studied in the zebrafish FOP model because of the advantages that the system offers. We can obtain existing zebrafish stocks that carry mutations in the same genes or design guide RNAs to target the genes of interest for CRISPR-mediated knockdown. We can quickly perform preliminary screens to evaluate the effects of each gene mutation on the embryonic development of *Tg(acvr1l_Q204D)* or *Tg(acvr1l_R203H)* zebrafish and then move interesting candidates into testing in adult animals. We are confident that these experiments will uncover new and exciting regulators of ACVR1 function in the context of FOP disease progression and may yield additional targets for therapeutics.

In conclusion, our work reveals the advantages and limitations of the first adult zebrafish model for FOP. Our future work will attempt to address these limitations, through the creation of animals harboring FOP patient-associated mutation, and through further investigation of the mechanisms of wound healing following injury in the zebrafish FOP model. We will also exploit the advantages of the zebrafish model to learn more about the genetic and molecular mechanisms driving FOP disease progression. It is

our hope that this continued work will uncover novel therapeutic opportunities and ultimately improve the quality and duration of life for human FOP patients.

Chapter 5: Bibliography

1. F. S. Kaplan, J. A. Tabas, F. H. Gannon, G. Finkel, G. V. Hahn, M. A. Zasloff, The histopathology of fibrodysplasia ossificans progressiva. An endochondral process, *J Bone Joint Surg Am* **75**, 220–230 (1993).

2. F. S. Kaplan, M. Le Merrer, D. L. Glaser, R. J. Pignolo, R. E. Goldsby, J. A. Kitterman, J. Groppe, E. M. Shore, Fibrodysplasia ossificans progressiva, *Best Pract Res Clin Rheumatol* **22**, 191–205 (2008).

3. M. Kartal-Kaess, E. M. Shore, M. Xu, L. Schwering, M. Uhl, R. Korinthenberg, C. Niemeyer, F. S. Kaplan, M. Lauten, Fibrodysplasia ossificans progressiva (FOP): watch the great toes! *Eur. J. Pediatr.* **169**, 1417–1421 (2010).

4. R. J. Pignolo, E. M. Shore, F. S. Kaplan, Fibrodysplasia ossificans progressiva: clinical and genetic aspects, *Orphanet J Rare Dis* **6**, 80 (2011).

5. F. S. Kaplan, S. A. Chakkalakal, E. M. Shore, Fibrodysplasia ossificans progressiva: mechanisms and models of skeletal metamorphosis, *Dis Model Mech* **5**, 756–762 (2012).

6. E. F. McCarthy, M. Sundaram, Heterotopic ossification: a review, *Skeletal Radiol.* **34**, 609–619 (2005).

7. E. M. Shore, M. Xu, G. J. Feldman, D. A. Fenstermacher, T.-J. Cho, I. H. Choi, J. M. Connor, P. Delai, D. L. Glaser, M. LeMerrer, R. Morhart, J. G. Rogers, R. Smith, J. T. Triffitt, J. A. Urtizberea, M. Zasloff, M. A. Brown, F. S. Kaplan, A recurrent mutation in the BMP type I receptor ACVR1 causes inherited and sporadic fibrodysplasia ossificans progressiva, *Nat. Genet.* **38**, 525–527 (2006).

8. F. S. Kaplan, M. Xu, P. Seemann, J. M. Connor, D. L. Glaser, L. Carroll, P. Delai, E. Fastnacht-Urban, S. J. Forman, G. Gillessen-Kaesbach, J. Hoover-Fong, B. Köster, R. M. Pauli, W. Reardon, S.-A. Zaidi, M. Zasloff, R. Morhart, S. Mundlos, J. Groppe, E. M. Shore, Classic and atypical fibrodysplasia ossificans progressiva (FOP) phenotypes are caused by mutations in the bone morphogenetic protein (BMP) type I receptor ACVR1, *Hum. Mutat.* **30**, 379–390 (2009).

9. P. C. Billings, J. L. Fiori, J. L. Bentwood, M. P. O'Connell, X. Jiao, B. Nussbaum, R. J. Caron, E. M. Shore, F. S. Kaplan, Dysregulated BMP Signaling and Enhanced Osteogenic Differentiation of Connective Tissue Progenitor Cells From Patients With Fibrodysplasia Ossificans Progressiva (FOP), *J. Bone Miner. Res.* **23**, 305–313 (2008).

10. T. Fukuda, M. Kohda, K. Kanomata, J. Nojima, A. Nakamura, J. Kamizono, Y. Noguchi, K. Iwakiri, T. Kondo, J. Kurose, K.-I. Endo, T. Awakura, J. Fukushi, Y. Nakashima, T. Chiyonobu, A. Kawara, Y. Nishida, I. Wada, M. Akita, T. Komori, K. Nakayama, A. Nanba, Y. Maruki, T. Yoda, H. Tomoda, P. B. Yu, E. M. Shore, F. S. Kaplan, K. Miyazono, M. Matsuoka, K. Ikebuchi, A. Ohtake, H. Oda, E. Jimi, I. Owan, Y. Okazaki, T. Katagiri, Constitutively activated ALK2 and increased SMAD1/5 cooperatively induce bone morphogenetic protein signaling in fibrodysplasia ossificans

progressiva, *J. Biol. Chem.* **284**, 7149–7156 (2009).

11. M. van Dinther, N. Visser, D. J. J. de Gorter, J. Doorn, M.-J. Goumans, J. de Boer, P. ten Dijke, ALK2 R206H mutation linked to fibrodysplasia ossificans progressiva confers constitutive activity to the BMP type I receptor and sensitizes mesenchymal cells to BMP-induced osteoblast differentiation and bone formation, *J. Bone Miner. Res.* **25**, 1208–1215 (2010).

12. A. L. Culbert, S. A. Chakkalakal, E. G. Theosmy, T. A. Brennan, F. S. Kaplan, E. M. Shore, Alk2 regulates early chondrogenic fate in fibrodysplasia ossificans progressiva heterotopic endochondral ossification, *Stem Cells* **32**, 1289–1300 (2014).

13. J. Haupt, A. Deichsel, K. Stange, C. Ast, R. Bocciardi, R. Ravazzolo, M. Di Rocco, P. Ferrari, A. Landi, F. S. Kaplan, E. M. Shore, C. Reissner, P. Seemann, ACVR1 p.Q207E causes classic fibrodysplasia ossificans progressiva and is functionally distinct from the engineered constitutively active ACVR1 p.Q207D variant, *Hum. Mol. Genet.* (2014), doi:10.1093/hmg/ddu255.

14. R. B. Cohen, G. V. Hahn, J. A. Tabas, J. Peeper, C. L. Levitz, A. Sando, N. Sando, M. Zasloff, F. S. Kaplan, The natural history of heterotopic ossification in patients who have fibrodysplasia ossificans progressiva. A study of forty-four patients, *J Bone Joint Surg Am* **75**, 215–219 (1993).

15. D. M. Rocke, M. Zasloff, J. Peeper, R. B. Cohen, F. S. Kaplan, Age- and joint-specific risk of initial heterotopic ossification in patients who have fibrodysplasia ossificans progressiva, *Clinical Orthopaedics and Related Research*, 243–248 (1994).

16. R. J. Pignolo, C. Bedford-Gay, M. Liljesthröm, B. P. Durbin-Johnson, E. M. Shore, D. M. Rocke, F. S. Kaplan, The Natural History of Flare-Ups in Fibrodysplasia Ossificans Progressiva (FOP): A Comprehensive Global Assessment, *J. Bone Miner. Res.* **31**, 650–656 (2016).

17. F. S. Kaplan, M. A. Zasloff, J. A. Kitterman, E. M. Shore, Early mortality and cardiorespiratory failure in patients with fibrodysplasia ossificans progressiva, *J Bone Joint Surg …* (2010).

18. S. J. Hatsell, V. Idone, D. M. A. Wolken, L. Huang, H. J. Kim, L. Wang, X. Wen, K. C. Nannuru, J. Jimenez, L. Xie, N. Das, G. Makhoul, R. Chernomorsky, D. D'Ambrosio, R. A. Corpina, C. J. Schoenherr, K. Feeley, P. B. Yu, G. D. Yancopoulos, A. J. Murphy, A. N. Economides, ACVR1R206H receptor mutation causes fibrodysplasia ossificans progressiva by imparting responsiveness to activin A, *Sci Transl Med* **7**, 303ra137–303ra137 (2015).

19. A. Yabuzoe, S.-I. Yokoi, M. Sekiguchi, Y. Momoi, K. Ide, K. Nishifuji, T. Iwasaki, Fibrodysplasia ossificans progressiva in a Maine Coon cat with prominent ossification in dorsal muscle, *J. Vet. Med. Sci.* **71**, 1649–1652 (2009).

20. L. F. La Sala, L. M. Pozzi, D. McAloose, F. S. Kaplan, E. M. Shore, E. J. O.

Kompanje, I. F. Sidor, L. Musmeci, M. M. Uhart, Severe soft tissue ossification in a southern right whale Eubalaena australis, *Dis. Aquat. Org.* **102**, 149–156 (2012).

21. M. LaBonty, P. C. Yelick, Animal models of fibrodysplasia ossificans progressiva, *Dev. Dyn.* **247**, 279–288 (2018).

22. J. A. Kitterman, J. B. Strober, L. Kan, D. M. Rocke, A. Cali, J. Peeper, J. Snow, P. L. R. Delai, R. Morhart, R. J. Pignolo, E. M. Shore, F. S. Kaplan, Neurological symptoms in individuals with fibrodysplasia ossificans progressiva, *J. Neurol.* **259**, 2636–2643 (2012).

23. J. Massagué, TGF-beta signal transduction, *Annu. Rev. Biochem.* **67**, 753–791 (1998).

24. R. Derynck, Y. E. Zhang, Smad-dependent and Smad-independent pathways in TGF-beta family signalling, *Nature* **425**, 577–584 (2003).

25. T. D. Mueller, Mechanisms of BMP-Receptor Interaction and Activation, *Vitam. Horm.* **99**, 1–61 (2015).

26. M. Y. Wu, C. S. Hill, Tgf-beta superfamily signaling in embryonic development and homeostasis, *Dev. Cell* **16**, 329–343 (2009).

27. M. Wu, G. Chen, Y.-P. Li, TGF-β and BMP signaling in osteoblast, skeletal development, and bone formation, homeostasis and disease, *Bone Res* **4**, 16009 (2016).

28. M. Macías-Silva, P. A. Hoodless, S. J. Tang, M. Buchwald, J. L. Wrana, Specific activation of Smad1 signaling pathways by the BMP7 type I receptor, ALK2, *J. Biol. Chem.* **273**, 25628–25636 (1998).

29. M. S. Rahman, N. Akhtar, H. M. Jamil, R. S. Banik, S. M. Asaduzzaman, TGF-β/BMP signaling and other molecular events: regulation of osteoblastogenesis and bone formation, *Bone Res* **3**, 15005 (2015).

30. Y. G. Chen, J. Massagué, Smad1 recognition and activation by the ALK1 group of transforming growth factor-beta family receptors, *J. Biol. Chem.* **274**, 3672–3677 (1999).

31. M. P. Hedger, W. R. Winnall, D. J. Phillips, D. M. de Kretser, The regulation and functions of activin and follistatin in inflammation and immunity, *Vitam. Horm.* **85**, 255–297 (2011).

32. O. E. Olsen, K. F. Wader, H. Hella, A. K. Mylin, I. Turesson, I. Nesthus, A. Waage, A. Sundan, T. Holien, Activin A inhibits BMP-signaling by binding ACVR2A and ACVR2B, *Cell Commun. Signal* **13**, 27 (2015).

33. P. B. Yu, D. Y. Deng, C. S. Lai, C. C. Hong, G. D. Cuny, M. L. Bouxsein, D. W. Hong, P. M. McManus, T. Katagiri, C. Sachidanandan, N. Kamiya, T. Fukuda, Y. Mishina, R. T. Peterson, K. D. Bloch, BMP type I receptor inhibition reduces heterotopic [corrected] ossification, *Nat. Med.* **14**, 1363–1369 (2008).

34. K. Hino, M. Ikeya, K. Horigome, Y. Matsumoto, H. Ebise, M. Nishio, K. Sekiguchi, M. Shibata, S. Nagata, S. Matsuda, J. Toguchida, Neofunction of ACVR1 in fibrodysplasia ossificans progressiva, *Proc. Natl. Acad. Sci. U.S.A.* **112**, 201510540–15443 (2015).

35. J. Bagarova, A. J. Vonner, K. A. Armstrong, J. Börgermann, C. S. C. Lai, D. Y. Deng, H. Beppu, I. Alfano, P. Filippakopoulos, N. W. Morrell, A. N. Bullock, P. Knaus, Y. Mishina, P. B. Yu, Constitutively active ALK2 receptor mutants require type II receptor cooperation, *Mol. Cell. Biol.* **33**, 2413–2424 (2013).

36. V. Q. Le, K. A. Wharton, A. Singh, K. D. Irvine, Eds. Hyperactive BMP signaling induced by ALK2(R206H) requires type II receptor function in a Drosophila model for classic fibrodysplasia ossificans progressiva, *Dev. Dyn.* **241**, 200–214 (2012).

37. J. C. Groppe, E. M. Shore, F. S. Kaplan, Functional modeling of the ACVR1 (R206H) mutation in FOP, *Clinical Orthopaedics and Related Research* **462**, 87–92 (2007).

38. S. A. Chakkalakal, D. Zhang, A. L. Culbert, M. R. Convente, R. J. Caron, A. C. Wright, A. D. A. Maidment, F. S. Kaplan, E. M. Shore, An Acvr1 R206H knock-in mouse has fibrodysplasia ossificans progressiva, *J. Bone Miner. Res.* **27**, 1746–1756 (2012).

39. E. M. Shore, F. S. Kaplan, Inherited human diseases of heterotopic bone formation, *Nat Rev Rheumatol* **6**, 518–527 (2010).

40. T. F. Lanchoney, R. B. Cohen, D. M. Rocke, M. A. Zasloff, F. S. Kaplan, Permanent heterotopic ossification at the injection site after diphtheria-tetanus-pertussis immunizations in children who have fibrodysplasia ossificans progressiva, *The Journal of Pediatrics* **126**, 762–764 (1995).

41. R. F. Scarlett, D. M. Rocke, S. Kantanie, J. B. Patel, E. M. Shore, F. S. Kaplan, Influenza-like Viral Illnesses and Flare-ups of Fibrodysplasia Ossificans Progressiva, *Clinical Orthopaedics and Related Research* **423**, 275–279 (2004).

42. F. H. Gannon, B. A. Valentine, E. M. Shore, M. A. Zasloff, F. S. Kaplan, Acute Lymphocytic Infiltration in an Extremely Early Lesion of Fibrodysplasia Ossificans Progressiva, *Clinical Orthopaedics and Related Research* **346**, 19 (1998).

43. F. H. Gannon, D. Glaser, R. Caron, L. D. R. Thompson, E. M. Shore, F. S. Kaplan, Mast cell involvement in fibrodysplasia ossificans progressiva, *Human Pathology* **32**, 842–848 (2001).

44. F. S. Kaplan, E. M. Shore, R. Gupta, P. C. Billings, D. L. Glaser, R. J. Pignolo, D. Graf, M. Kamoun, Immunological features of fibrodysplasia ossificans progressiva and the dysregulated BMP4 pathway, *Clinic Rev Bone Miner Metab* **3**, 189–193 (2005).

45. F. S. Kaplan, D. L. Glaser, E. M. Shore, R. J. Pignolo, M. Xu, Y. Zhang, D. Senitzer,

S. J. Forman, S. G. Emerson, Hematopoietic stem-cell contribution to ectopic skeletogenesis, *J Bone Joint Surg Am* **89**, 347–357 (2007).

46. L. Kan, Y. Liu, T. L. McGuire, D. M. P. Berger, R. B. Awatramani, S. M. Dymecki, J. A. Kessler, Dysregulation of local stem/progenitor cells as a common cellular mechanism for heterotopic ossification, *Stem Cells* **27**, 150–156 (2009).

47. D. Dey, J. Bagarova, S. J. Hatsell, K. A. Armstrong, L. Huang, J. Ermann, A. J. Vonner, Y. Shen, A. H. Mohedas, A. Lee, E. M. W. Eekhoff, A. van Schie, M. B. Demay, C. Keller, A. J. Wagers, A. N. Economides, P. B. Yu, Two tissue-resident progenitor lineages drive distinct phenotypes of heterotopic ossification, *Sci Transl Med* **8**, 366ra163–366ra163 (2016).

48. L. Kan, C.-Y. Peng, T. L. McGuire, J. A. Kessler, Glast-expressing progenitor cells contribute to heterotopic ossification, *Bone* **53**, 194–203 (2013).

49. V. Y. Lounev, R. Ramachandran, M. N. Wosczyna, M. Yamamoto, A. D. A. Maidment, E. M. Shore, D. L. Glaser, D. J. Goldhamer, F. S. Kaplan, Identification of progenitor cells that contribute to heterotopic skeletogenesis, *J Bone Joint Surg Am* **91**, 652–663 (2009).

50. D. Medici, E. M. Shore, V. Y. Lounev, F. S. Kaplan, R. Kalluri, B. R. Olsen, Conversion of vascular endothelial cells into multipotent stem-like cells, *Nat. Med.* **16**, 1400–1406 (2010).

51. M. N. Wosczyna, A. A. Biswas, C. A. Cogswell, D. J. Goldhamer, Multipotent progenitors resident in the skeletal muscle interstitium exhibit robust BMP-dependent osteogenic activity and mediate heterotopic ossification, *J. Bone Miner. Res.* **27**, 1004–1017 (2012).

52. R. K. Suda, P. C. Billings, K. P. Egan, J.-H. Kim, R. McCarrick-Walmsley, D. L. Glaser, D. L. Porter, E. M. Shore, R. J. Pignolo, Circulating osteogenic precursor cells in heterotopic bone formation, *Stem Cells* **27**, 2209–2219 (2009).

53. A. Al Kaissi, V. Kenis, M. Ben Ghachem, J. Hofstaetter, F. Grill, R. Ganger, S. G. Kircher, The Diversity of the Clinical Phenotypes in Patients With Fibrodysplasia Ossificans Progressiva, *Journal of Clinical Medicine Research* **8**, 246–253 (2016).

54. M. Pacifici, G. Cossu, M. Molinaro, F. Tato, Vitamin A inhibits chondrogenesis but not myogenesis, *Exp. Cell Res.* **129**, 469–474 (1980).

55. K. Shimono, W.-E. Tung, C. Macolino, A. H.-T. Chi, J. H. Didizian, C. Mundy, R. A. Chandraratna, Y. Mishina, M. Enomoto-Iwamoto, M. Pacifici, M. Iwamoto, Potent inhibition of heterotopic ossification by nuclear retinoic acid receptor-γ agonists, *Nat. Med.* **17**, 454–460 (2011).

56. S. A. Chakkalakal, K. Uchibe, M. R. Convente, D. Zhang, A. N. Economides, F. S. Kaplan, M. Pacifici, M. Iwamoto, E. M. Shore, Palovarotene Inhibits Heterotopic

Ossification and Maintains Limb Mobility and Growth in Mice With the Human ACVR1R206H Fibrodysplasia Ossificans Progressiva (FOP) Mutation, *J. Bone Miner. Res.* **31**, 1666–1675 (2016).

57. H. B. Warren, J. L. Carpenter, Fibrodysplasia ossificans in three cats, *Vet. Pathol.* **21**, 495–499 (1984).

58. B. A. Valentine, C. George, J. F. Randolph, S. A. Center, L. Fuhrer, K. A. Beck, Fibrodysplasia ossificans progressiva in the cat. A case report, *J. Vet. Intern. Med.* **6**, 335–340 (1992).

59. K. Asano, A. Sakata, H. Shibuya, M. Kitagawa, K. Teshima, Y. Kato, Y. Sasaki, K. Kutara, M. Seki, K. Edamura, T. Sato, S. Tanaka, Fibrodysplasia ossificans progressiva-like condition in a cat, *J. Vet. Med. Sci.* **68**, 1003–1006 (2006).

60. A. Klang, S. Kneissl, R. Glänzel, A. Fuchs-Baumgartinger, Imaging diagnosis: fibrodysplasia ossificans progressiva in a cat, *Vet Radiol Ultrasound* **54**, 532–535 (2013).

61. M. J. Guilliard, Fibrodysplasia ossificans in a German shepherd dog, *J Small Anim Pract* **42**, 550–553 (2001).

62. H. R. Seibold, C. L. Davis, Generalized myositis ossificans (familial) in pigs, *Pathol Vet* **4**, 79–88 (1967).

63. T. J. Brummel, V. Twombly, G. Marqués, J. L. Wrana, S. J. Newfeld, L. Attisano, J. Massagué, M. B. O'Connor, W. M. Gelbart, Characterization and relationship of Dpp receptors encoded by the saxophone and thick veins genes in Drosophila, *Cell* **78**, 251–261 (1994).

64. V. Twombly, E. Bangi, V. Le, B. Malnic, M. A. Singer, K. A. Wharton, Functional analysis of saxophone, the Drosophila gene encoding the BMP type I receptor ortholog of human ALK1/ACVRL1 and ACVR1/ALK2, *Genetics* **183**, 563–79– 1SI–8SI (2009).

65. P. C. Yelick, T. S. Abduljabbar, P. Stashenko, zALK-8, a novel type I serine/threonine kinase receptor, is expressed throughout early zebrafish development, *Dev. Dyn.* **211**, 352–361 (1998).

66. T. Xie, A. L. Finelli, R. W. Padgett, The Drosophila saxophone gene: a serine-threonine kinase receptor of the TGF-beta superfamily, *Science* **263**, 1756–1759 (1994).

67. A. Penton, Y. Chen, K. Staehling-Hampton, J. L. Wrana, L. Attisano, J. Szidonya, J. A. Cassill, J. Massagué, F. M. Hoffmann, Identification of two bone morphogenetic protein type I receptors in Drosophila and evidence that Brk25D is a decapentaplegic receptor, *Cell* **78**, 239–250 (1994).

68. D. Nellen, M. Affolter, K. Basler, Receptor serine/threonine kinases implicated in the control of Drosophila body pattern by decapentaplegic, *Cell* **78**, 225–237 (1994).

69. J. L. Neul, E. L. Ferguson, Spatially restricted activation of the SAX receptor by SCW modulates DPP/TKV signaling in Drosophila dorsal-ventral patterning, *Cell* **95**, 483–494 (1998).

70. E. L. Ferguson, K. V. Anderson, Decapentaplegic acts as a morphogen to organize dorsal-ventral pattern in the Drosophila embryo, *Cell* **71**, 451–461 (1992).

71. K. A. Wharton, R. P. Ray, W. M. Gelbart, An activity gradient of decapentaplegic is necessary for the specification of dorsal pattern elements in the Drosophila embryo, *Development* **117**, 807–822 (1993).

72. F. A. Spencer, F. M. Hoffmann, W. M. Gelbart, Decapentaplegic: a gene complex affecting morphogenesis in Drosophila melanogaster, *Cell* **28**, 451–461 (1982).

73. E. Bangi, K. Wharton, Dual function of the Drosophila Alk1/Alk2 ortholog Saxophone shapes the Bmp activity gradient in the wing imaginal disc, *Development* **133**, 3295–3303 (2006).

74. R. W. Padgett, J. M. Wozney, W. M. Gelbart, Human BMP sequences can confer normal dorsal-ventral patterning in the Drosophila embryo, *Proc. Natl. Acad. Sci. U.S.A.* **90**, 2905–2909 (1993).

75. Z. Gu, E. M. Reynolds, J. Song, H. Lei, A. Feijen, L. Yu, W. He, D. T. MacLaughlin, J. van den Eijnden-van Raaij, P. K. Donahoe, E. Li, The type I serine/threonine kinase receptor ActRIA (ALK2) is required for gastrulation of the mouse embryo, *Development* **126**, 2551–2561 (1999).

76. H. Beppu, M. Kawabata, T. Hamamoto, A. Chytil, O. Minowa, T. Noda, K. Miyazono, BMP type II receptor is required for gastrulation and early development of mouse embryos, *Dev. Biol.* **221**, 249–258 (2000).

77. V. Kaartinen, M. Dudas, A. Nagy, S. Sridurongrit, M. M. Lu, J. A. Epstein, Cardiac outflow tract defects in mice lacking ALK2 in neural crest cells, *Development* **131**, 3481–3490 (2004).

78. M. Dudas, S. Sridurongrit, A. Nagy, K. Okazaki, V. Kaartinen, Craniofacial defects in mice lacking BMP type I receptor Alk2 in neural crest cells, *Mech. Dev.* **121**, 173–182 (2004).

79. S. M. C. de Sousa Lopes, B. A. J. Roelen, R. M. Monteiro, R. Emmens, H. Y. Lin, E. Li, K. A. Lawson, C. L. Mummery, BMP signaling mediated by ALK2 in the visceral endoderm is necessary for the generation of primordial germ cells in the mouse embryo, *Genes Dev.* **18**, 1838–1849 (2004).

80. R. Rajagopal, L. K. Dattilo, V. Kaartinen, C.-X. Deng, L. Umans, A. Zwijsen, A. B. Roberts, E. P. Bottinger, D. C. Beebe, Functions of the type 1 BMP receptor Acvr1 (Alk2) in lens development: cell proliferation, terminal differentiation, and survival, *Invest. Ophthalmol. Vis. Sci.* **49**, 4953–4960 (2008).

81. R. U. de Iongh, Y. Chen, M. I. Kokkinos, J. W. McAvoy, BMP and activin receptor expression in lens development, *Mol. Vis.* **10**, 566–576 (2004).

82. T. Fukuda, G. Scott, Y. Komatsu, R. Araya, M. Kawano, M. K. Ray, M. Yamada, Y. Mishina, Generation of a mouse with conditionally activated signaling through the BMP receptor, ALK2, *Genesis* **44**, 159–167 (2006).

83. R. Wieser, J. L. Wrana, J. Massagué, GS domain mutations that constitutively activate T beta R-I, the downstream signaling component in the TGF-beta receptor complex, *EMBO J.* **14**, 2199–2208 (1995).

84. H. Wang, C. Lindborg, V. Lounev, J.-H. Kim, R. McCarrick-Walmsley, M. Xu, L. Mangiavini, J. C. Groppe, E. M. Shore, E. Schipani, F. S. Kaplan, R. J. Pignolo, Cellular Hypoxia Promotes Heterotopic Ossification by Amplifying BMP Signaling, *J. Bone Miner. Res.* **31**, 1652–1665 (2016).

85. J. Upadhyay, L. Xie, L. Huang, N. Das, R. C. Stewart, M. C. Lyon, K. Palmer, S. Rajamani, C. Graul, M. Lobo, T. J. Wellman, E. J. Soares, M. D. Silva, J. Hesterman, L. Wang, X. Wen, X. Qian, K. Nannuru, V. Idone, A. J. Murphy, A. N. Economides, S. J. Hatsell, The Expansion of Heterotopic Bone in Fibrodysplasia Ossificans Progressiva is Activin A-Dependent, *J. Bone Miner. Res.* (2017), doi:10.1002/jbmr.3235.

86. S. Agarwal, S. J. Loder, D. Cholok, J. Peterson, J. Li, C. Breuler, R. Cameron Brownley, H. Hsin Sung, M. T. Chung, N. Kamiya, S. Li, B. Zhao, V. Kaartinen, T. A. Davis, A. T. Qureshi, E. Schipani, Y. Mishina, B. Levi, Scleraxis-Lineage Cells Contribute to Ectopic Bone Formation in Muscle and Tendon, *Stem Cells* **35**, 705–710 (2017).

87. T. L. Payne, J. H. Postlethwait, P. C. Yelick, Functional characterization and genetic mapping of alk8, *Mech. Dev.* **100**, 275–289 (2001).

88. H. Bauer, Z. Lele, G. J. Rauch, R. Geisler, M. Hammerschmidt, The type I serine/threonine kinase receptor Alk8/Lost-a-fin is required for Bmp2b/7 signal transduction during dorsoventral patterning of the zebrafish embryo, *Development* **128**, 849–858 (2001).

89. K. A. Mintzer, M. A. Lee, G. Runke, J. Trout, M. Whitman, M. C. Mullins, Lost-a-fin encodes a type I BMP receptor, Alk8, acting maternally and zygotically in dorsoventral pattern formation, *Development* **128**, 859–869 (2001).

90. Q. Shen, S. C. Little, M. Xu, J. Haupt, C. Ast, T. Katagiri, S. Mundlos, P. Seemann, F. S. Kaplan, M. C. Mullins, E. M. Shore, The fibrodysplasia ossificans progressiva R206H ACVR1 mutation activates BMP-independent chondrogenesis and zebrafish embryo ventralization, *J. Clin. Invest.* **119**, 3462–3472 (2009).

91. M. LaBonty, N. Pray, P. C. Yelick, A Zebrafish Model of Human Fibrodysplasia Ossificans Progressiva, *Zebrafish* **14**, 293–304 (2017).

92. C. B. Kimmel, W. W. Ballard, S. R. Kimmel, B. Ullmann, T. F. Schilling, Stages of embryonic development of the zebrafish, *Dev. Dyn.* **203**, 253–310 (1995).

93. N. D. Meeker, N. S. Trede, Immunology and zebrafish: spawning new models of human disease, *Dev. Comp. Immunol.* **32**, 745–757 (2008).

94. F. S. Kaplan, R. J. Pignolo, E. M. Shore, Granting Immunity to FOP and Catching Heterotopic Ossification in the Act, *Semin. Cell Dev. Biol.* (2015), doi:10.1016/j.semcdb.2015.12.013.

95. K. Howe, M. D. Clark, C. F. Torroja, J. Torrance, C. Berthelot, M. Muffato, J. E. Collins, S. Humphray, K. McLaren, L. Matthews, S. McLaren, I. Sealy, M. Caccamo, C. Churcher, C. Scott, J. C. Barrett, R. Koch, G.-J. Rauch, S. White, W. Chow, B. Kilian, L. T. Quintais, J. A. Guerra-Assunção, Y. Zhou, Y. Gu, J. Yen, J.-H. Vogel, T. Eyre, S. Redmond, R. Banerjee, J. Chi, B. Fu, E. Langley, S. F. Maguire, G. K. Laird, D. Lloyd, E. Kenyon, S. Donaldson, H. Sehra, J. Almeida-King, J. Loveland, S. Trevanion, M. Jones, M. Quail, D. Willey, A. Hunt, J. Burton, S. Sims, K. McLay, B. Plumb, J. Davis, C. Clee, K. Oliver, R. Clark, C. Riddle, D. Eliott, G. Threadgold, G. Harden, D. Ware, B. Mortimer, G. Kerry, P. Heath, B. Phillimore, A. Tracey, N. Corby, M. Dunn, C. Johnson, J. Wood, S. Clark, S. Pelan, G. Griffiths, M. Smith, R. Glithero, P. Howden, N. Barker, C. Stevens, J. Harley, K. Holt, G. Panagiotidis, J. Lovell, H. Beasley, C. Henderson, D. Gordon, K. Auger, D. Wright, J. Collins, C. Raisen, L. Dyer, K. Leung, L. Robertson, K. Ambridge, D. Leongamornlert, S. McGuire, R. Gilderthorp, C. Griffiths, D. Manthravadi, S. Nichol, G. Barker, S. Whitehead, M. Kay, J. Brown, C. Murnane, E. Gray, M. Humphries, N. Sycamore, D. Barker, D. Saunders, J. Wallis, A. Babbage, S. Hammond, M. Mashreghi-Mohammadi, L. Barr, S. Martin, P. Wray, A. Ellington, N. Matthews, M. Ellwood, R. Woodmansey, G. Clark, J. Cooper, A. Tromans, D. Grafham, C. Skuce, R. Pandian, R. Andrews, E. Harrison, A. Kimberley, J. Garnett, N. Fosker, R. Hall, P. Garner, D. Kelly, C. Bird, S. Palmer, I. Gehring, A. Berger, C. M. Dooley, Z. Ersan-Ürün, C. Eser, H. Geiger, M. Geisler, L. Karotki, A. Kirn, J. Konantz, M. Konantz, M. Oberländer, S. Rudolph-Geiger, M. Teucke, K. Osoegawa, B. Zhu, A. Rapp, S. Widaa, C. Langford, F. Yang, N. P. Carter, J. Harrow, Z. Ning, J. Herrero, S. M. J. Searle, A. Enright, R. Geisler, R. H. A. Plasterk, C. Lee, M. Westerfield, P. J. de Jong, L. I. Zon, J. H. Postlethwait, C. Nüsslein-Volhard, T. J. P. Hubbard, H. R. Crollius, J. Rogers, D. L. Stemple, The zebrafish reference genome sequence and its relationship to the human genome, *Nature* **496**, 498–503 (2013).

96. L. Solnica-Krezel, A. F. Schier, W. Driever, Efficient recovery of ENU-induced mutations from the zebrafish germline, *Genetics* **136**, 1401–1420 (1994).

97. K. Kawakami, Transgenesis and gene trap methods in zebrafish by using the Tol2 transposable element, *Methods Cell Biol.* **77**, 201–222 (2004).

98. S. Albadri, F. Del Bene, C. Revenu, Genome editing using CRISPR/Cas9-based knock-in approaches in zebrafish, *Methods* **121-122**, 77–85 (2017).

99. F. S. Kaplan, M. Al Mukaddam, R. J. Pignolo, A cumulative analogue joint

involvement scale (CAJIS) for fibrodysplasia ossificans progressiva (FOP), *Bone* **101**, 123–128 (2017).

100. R. M. White, A. Sessa, C. Burke, T. Bowman, J. LeBlanc, C. Ceol, C. Bourque, M. Dovey, W. Goessling, C. E. Burns, L. I. Zon, Transparent Adult Zebrafish as a Tool for In Vivo Transplantation Analysis, *Cell Stem Cell* **2**, 183–189 (2008).

101. W. Shoji, M. Sato-Maeda, Application of heat shock promoter in transgenic zebrafish, *Dev. Growth Differ.* **50**, 401–406 (2008).

102. A. Felker, C. Mosimann, in *The Zebrafish - Genetics, Genomics, and Transcriptomics*, Methods in Cell Biology. (Elsevier, 2016), vol. 135, pp. 219–244.

103. W. P. Dempsey, S. E. Fraser, P. Pantazis, PhOTO zebrafish: a transgenic resource for in vivo lineage tracing during development and regeneration, *PLoS ONE* **7**, e32888 (2012).

104. C. A. MacRae, R. T. Peterson, Zebrafish as tools for drug discovery, *Nat Rev Drug Discov* **14**, 721–731 (2015).

105. L. Hildebrand, K. Stange, A. Deichsel, M. Gossen, P. Seemann, The Fibrodysplasia Ossificans Progressiva (FOP) mutation p.R206H in ACVR1 confers an altered ligand response, *Cell. Signal.* (2016), doi:10.1016/j.cellsig.2016.10.001.

106. R. J. Duszynski, J. Topczewski, E. E. LeClair, Simple, economical heat-shock devices for zebrafish housing racks, *Zebrafish* **8**, 211–219 (2011).

107. M. Westerfield, *The zebrafish book* (A guide for laboratory use of zebrafish (Danio rerio), 1995).

108. C. Alexander, E. Zuniga, I. L. Blitz, N. Wada, P. Le Pabic, Y. Javidan, T. Zhang, K. W. Cho, J. G. Crump, T. F. Schilling, Combinatorial roles for BMPs and Endothelin 1 in patterning the dorsal-ventral axis of the craniofacial skeleton, *Development* **138**, 5135–5146 (2011).

109. K. M. Kwan, E. Fujimoto, C. Grabher, B. D. Mangum, M. E. Hardy, D. S. Campbell, J. M. Parant, H. J. Yost, J. P. Kanki, C.-B. Chien, The Tol2kit: a multisite gateway-based construction kit for Tol2 transposon transgenesis constructs, *Dev. Dyn.* **236**, 3088–3099 (2007).

110. M. H. Braun, S. L. Steele, S. F. Perry, The responses of zebrafish (Danio rerio) to high external ammonia and urea transporter inhibition: nitrogen excretion and expression of rhesus glycoproteins and urea transporter proteins, *J. Exp. Biol.* **212**, 3846–3856 (2009).

111. B. K. Hall, The role of movement and tissue interactions in the development and growth of bone and secondary cartilage in the clavicle of the embryonic chick, *J Embryol Exp Morphol* **93**, 133–152 (1986).

112. M. H. Connolly, P. C. Yelick, High-throughput methods for visualizing the teleost skeleton: capturing autofluorescence of alizarin red, *Journal of Applied Ichthyology* **26**, 274–277 (2010).

113. C. W. Boswell, B. Ciruna, Understanding Idiopathic Scoliosis: A New Zebrafish School of Thought, *Trends Genet.* **33**, 183–196 (2017).

114. J. A. Tucker, K. A. Mintzer, M. C. Mullins, The BMP signaling gradient patterns dorsoventral tissues in a temporally progressive manner along the anteroposterior axis, *Dev. Cell* **14**, 108–119 (2008).

115. M. Hammerschmidt, G. N. Serbedzija, A. P. McMahon, Genetic analysis of dorsoventral pattern formation in the zebrafish: requirement of a BMP-like ventralizing activity and its dorsal repressor, *Genes Dev.* **10**, 2452–2461 (1996).

116. L. Dale, F. C. Wardle, A gradient of BMP activity specifies dorsal-ventral fates in early Xenopus embryos, *Semin. Cell Dev. Biol.* **10**, 319–326 (1999).

117. M. P. de Caestecker, M. Bottomley, S. Bhattacharyya, T. L. Payne, A. B. Roberts, P. C. Yelick, The novel type I serine-threonine kinase receptor Alk8 binds TGF-beta in the presence of TGF-betaRII, *Biochem. Biophys. Res. Commun.* **293**, 1556–1565 (2002).

118. T. Nakamura, A. R. Gehrke, J. Lemberg, J. Szymaszek, N. H. Shubin, Digits and fin rays share common developmental histories, *Nature* **537**, 225–228 (2016).

119. H. Suzuki, Y. Ito, M. Shinohara, S. Yamashita, S. Ichinose, A. Kishida, T. Oyaizu, T. Kayama, R. Nakamichi, N. Koda, K. Yagishita, M. K. Lotz, A. Okawa, H. Asahara, Gene targeting of the transcription factor Mohawk in rats causes heterotopic ossification of Achilles tendon via failed tenogenesis, *Proc. Natl. Acad. Sci. U.S.A.* **113**, 7840–7845 (2016).

120. L. Kan, V. Y. Lounev, R. J. Pignolo, L. Duan, Y. Liu, S. R. Stock, T. L. McGuire, B. Lu, N. P. Gerard, E. M. Shore, F. S. Kaplan, J. A. Kessler, Substance P signaling mediates BMP-dependent heterotopic ossification, *J. Cell. Biochem.* **112**, 2759–2772 (2011).

121. K. Hino, K. Horigome, M. Nishio, S. Komura, S. Nagata, C. Zhao, Y. Jin, K. Kawakami, Y. Yamada, A. Ohta, J. Toguchida, M. Ikeya, Activin-A enhances mTOR signaling to promote aberrant chondrogenesis in fibrodysplasia ossificans progressiva, *J. Clin. Invest.* **127** (2017), doi:10.1172/JCI93521.

122. S. Agarwal, S. J. Loder, C. Breuler, J. Li, D. Cholok, C. Brownley, J. Peterson, H. H. Hsieh, J. Drake, K. Ranganathan, Y. S. Niknafs, W. Xiao, S. Li, R. Kumar, R. Tompkins, M. T. Longaker, T. A. Davis, P. B. Yu, Y. Mishina, B. Levi, Strategic Targeting of Multiple BMP Receptors Prevents Trauma-Induced Heterotopic Ossification, *Mol. Ther.* **25**, 1974–1987 (2017).

123. T. A. Brennan, C. M. Lindborg, C. R. Bergbauer, H. Wang, F. S. Kaplan, R. J.

Pignolo, Mast cell inhibition as a therapeutic approach in fibrodysplasia ossificans progressiva (FOP), *Bone* (2017), doi:10.1016/j.bone.2017.08.023.

124. C. Seger, M. Hargrave, X. Wang, R. J. Chai, S. Elworthy, P. W. Ingham, Analysis of Pax7 expressing myogenic cells in zebrafish muscle development, injury, and models of disease, *Dev. Dyn.* **240**, 2440–2451 (2011).

125. J. F. Webb, J. E. Shirey, Postembryonic development of the cranial lateral line canals and neuromasts in zebrafish, *Dev. Dyn.* **228**, 370–385 (2003).

126. G. Gabbiani, F. T. Bosman, I. Stamenkovic, Eds. The myofibroblast in wound healing and fibrocontractive diseases, *The Journal of Pathology* **200**, 500–503 (2003).

127. J. W. Penn, A. O. Grobbelaar, K. J. Rolfe, The role of the TGF-β family in wound healing, burns and scarring: a review, *Int J Burns Trauma* **2**, 18–28 (2012).

128. A. Jaźwińska, R. Badakov, M. T. Keating, Activin-betaA signaling is required for zebrafish fin regeneration, *Curr. Biol.* **17**, 1390–1395 (2007).

129. S. Y. Lin Shiau, M. C. Huang, C. Y. Lee, Mechanism of action of cobra cardiotoxin in the skeletal muscle, *J. Pharmacol. Exp. Ther.* **196**, 758–770 (1976).

130. D. M. Alessi Wolken, V. Idone, S. J. Hatsell, P. B. Yu, A. N. Economides, The obligatory role of Activin A in the formation of heterotopic bone in Fibrodysplasia Ossificans Progressiva, *Bone* (2017), doi:10.1016/j.bone.2017.06.011.

131. M. Gemberling, T. J. Bailey, D. R. Hyde, K. D. Poss, The zebrafish as a model for complex tissue regeneration, *Trends Genet.* **29**, 611–620 (2013).

132. N. Blum, G. Begemann, Retinoic acid signaling controls the formation, proliferation and survival of the blastema during adult zebrafish fin regeneration, *Development* **139**, 107–116 (2012).

133. A. D. Weston, L. M. Hoffman, T. M. Underhill, Revisiting the role of retinoid signaling in skeletal development, *Birth Defects Res. C Embryo Today* **69**, 156–173 (2003).

134. L. Hildebrand, K. Stange, A. Deichsel, M. Gossen, P. Seemann, The Fibrodysplasia Ossificans Progressiva (FOP) mutation p.R206H in ACVR1 confers an altered ligand response, *Cell. Signal.* **29**, 23–30 (2017).